STATUS REPORTS

To The

ENGINEERING PROJECT ADVISORY COMMITTEE

March 22, 1990
Institute of Paper Science and Technology
Atlanta, Georgia

STATUS REPORTS

To The

ENGINEERING PROJECT ADVISORY COMMITTEE

March 22, 1990
Institute of Paper Science and Technology
Atlanta, Georgia

March 1, 1990

TO: MEMBERS OF THE ENGINEERING PROJECT ADVISORY COMMITTEE

Attached for your review are the Status Reports for the projects to be discussed at the Engineering Project Advisory Committee meeting scheduled for March 22, 1990, in Atlanta. A meeting agenda can be found inside the booklet.

We look forward to seeing you on March 22. Best regards.

Sincerely yours,

Richard Ellis, Director
Engineering & Paper Materials Division

RE/at
Enclosure

Institute of Paper Science and Technology, Inc.

5[illegible] 14th Street, N.W.
Atlanta, GA 30318

Formerly The Institute of Paper Chemistry
Appleton, Wisconsin

Telephone 404-853-9500
FAX # 404-853-9510

TABLE OF CONTENTS

AGENDA

ENGINEERING PROJECT ADVISORY COMMITTEE

March 22, 1990
Institute of Paper Science and Technology
Georgia Power Technology Applications Center
Atlanta, Georgia

Thursday -- March 22

8:00 - 9:00	OPENING REMARK	Ronald A. Yeske
	PROJECT REVIEWS	
	Fundamentals of Corrosion Control in Paper Mills	Per-Erik Ahlers
	Recovery Boiler Fireside Corrosion	Per-Erik Ahlers
	Corrosion Control in Batch Digesters	Per-Erik Ahlers
	Fundamentals of Water Removal Processes	Jeffrey Lindsay
	Fundamentals of Coating Systems	Cyrus Aidun
	X-Ray Studies of Web Consolidation	Cyrus Aidun
12:00 - 1:00	LUNCH	
	Fundamentals of Drying	David Orloff

Friday -- March 23

8:00 - 12:00	Committee Meeting (IPST Conference Room) Tour of IRF

Engineering -- Project Advisory Committee

Dr. W.B.A. Sharp, Chairman - 6/90*
Group Leader
Westvaco Corporation
Laurel Research Center
11101 Johns Hopkins Road
Laurel, MD 20707
301/792-9100

Mr. Percy E. Brooks - 6/90
Manager, Pulp & Paper Engineering
Georgia - Pacific Corporation
133 Peachtree Street, NE
Post Office Box 105605
Atlanta, GA 30348-5605
404/521-4618

Mr. Richard J. Posey - 6/91
Technical Services Superintendent
Great Southern Paper Company
Post Office Box 44
Cedar Springs, GA 31732
912/372-5541

Mr. John K. Rogers - 6/92
Director, Manufacturing Technology
James River Corporation
1915 Marathon Avenue
Post Office Box 899
Neenah, WI 54956
203/438-6250

Dr. D. Angela Wensley - 6/91
Engineering Associate
MacMillan Bloedel, Inc.
3350 East Broadway
Vancouver, BC V5M 4E6
CANADA
604/254-5151

Mr. Sven S. Arenander - 6/90
Group Leader
Union Camp Corporation
Post Office Box 3301
Princeton, NJ 08543-3301
609/896-1200

Mr. David J. Lacz - 6/91
Senior Development Engineer
Eastman Kodak Company
Building 319
Kodak Park
Rochester, NY 14650
716/458-1000

Dr. Henry Luming - 6/91
Project Manager
Stone Container Corporation
616 Executive Drive
Willowbrook, IL 60521
312/655-6940

Mr. Pharat B. Shah - 6/91
Manager of Technical Services
Wisconsin Tissue Mills, Inc.
Post Office Box 489
Menasha, WI 54952
414/725-7031

2/26/90
*date of retirement

FUNDAMENTALS OF CORROSION CONTROL IN PAPER MILLS

STATUS REPORT

FOR

PROJECT 3309

March 22, 1990

Institute of Paper Science and Technology
Atlanta, Georgia

PROJECT SUMMARY FORM

DATE: March 5, 1990

PROJECT: 3309 - Fundamentals of Corrosion Control in Paper Mills

PROJECT LEADER: Per-Erik Ahlers

IPST GOAL:

Increase the useful life of equipment by proper selection of construction materials and by identifying suitable process conditions.

OBJECTIVE:

To improve the life of paper machine suction rolls through corrosion and corrosion fatigue studies to establish mechanisms that limit lifetime and to identify failure preventive measures.

CURRENT FISCAL BUDGET: $ 150,000

PRIOR RESULTS:

The fully reversed loading S-N tests have been of little value in differentiating between suction roll alloys. The near-threshold fatigue crack growth results of several suction roll alloys have been in accordance with their service performance characteristics. The latest results show that the new alloy 86 is at least as good as alloy 75. High residual stresses is found associated to repair weldings.

SUMMARY OF RESULTS SINCE LAST REPORT:

The activity was confined to work related to installation of the MTS machine, the fatigue machine, and the rotating bending machines (4). The MTS machine has been calibrated and put in order to be ready for immediate use. Laurent Vesier began to work in the corrosion group at the end of February. He has an M.S. degree in material engineering from Georgia Tech.,

where he conducted corrosion fatigue tests. Rotating bending tests conducted by Ross Huhn, an MS student, were continued to complete fatigue runs in air. He is ready to initiate the testing with concentrated metal chloride solutions. For the push pull machine, which is intended for studies of superimposed mean stresses, the "tailor made" grips are being plated with copper to get a good bond between its stainless steel parts. The low melting-point alloy used as bonding media will allow a stress-free installation of test specimens.

FUTURE PLANS:

Continue near threshold fatigue testing, complete the rotating bending fatigue testing, and investigate the effect of superimposed mean stresses.

FUNDAMENTALS OF CORROSION CONTROL IN PAPER MILLS
Project 3309

INTRODUCTION

The main target for the studies with suction roll alloys has been to develop a reliable laboratory testing method for special alloys in order to be able to predict the performance behavior and direct development of resistive new alloy to corrosion fatigue.

Different methods have been employed, such as fatigue life time tests (S-N tests) using R.R. Moore's rotating bending machine and near-threshold fatigue crack growth testing with MTS machine using pre-cracked compact specimens.

The rotating bending method has not appeared to be successful in predicting the life cycle for alloys. The results obtained have not been in agreement with mill practice. In service alloy 63, an austenitic molybdenum bearing stainless steel, has performed worse than alloy 75, a duplex stainless steel, whereas no difference in the fatigue life is found in the laboratory corrosion fatigue tests conducted in aggressive white water environments. Even notched specimens did not give any difference in the life times for the two alloy tested.

Corrosion fatigue is a joint effect between cyclic straining and chemical effect. When mechanical fatigue alone is in effect, the fatigue life depends on the metallurgical state of the alloy and of the stress amplitude. When the stress amplitude is below a critical level, the time to fracture will be indefinitely long. The threshold stress intensity range (ΔK_{th}) represents an important parameter in fatigue testing. K, the stress intensity factor, is an single parameter used to describe stress conditions at the crack tip and is direct proportional to the applied stress and square root of the crack length:

$$K = k\, S\, a^{-1/2},$$

where k is a combined material and crack form coefficient, S is the applied stress and "a" the crack length. Under constant stress conditions, thus, K is defined by the length of the defect in the material.

In fatigue testing, the stress load is varying cyclically between two extremity values K_{max} - K_{min} or ΔK. ΔK is used to describe the stress field at the crack tip area. Aggressive environment lowers the critical ΔK (ΔK_{th}). The most pronounced effect may be found with environments causing a highly local type of corrosion such as pitting or grain boundary attack because the by corrosion caused surface defects act as stress raisers.

A recent published article from Japan gave results of a study on the effect of growing pit size on the fatigue process (Y. Kongo; Corrosion-Vol. 45, No. 1,1989, p.7-11). The article hypothesizes that the corrosion fatigue process is composed of three stages: 1) pit initiation and growth, 2) crack formation from the pit bottoms, and 3) crack propagation. During the first stage the ΔK is still below the threshold value which is reached in the second stages. The last phase is almost a pure mechanical process when high frequency is employed.

Looking at our previous results from corrosion fatigue studies near the threshold stress intensity range (ΔK_{th}), it is seen that the ΔK_{th} values are not greatly affected by the test environment unless the pH value is below 3.5 (Report by R. Yeske included the previous status report). At a pH value of 1 the threshold ΔK values were significantly lower than at pH 3.5. pH 2.5 is known to be a critical value in many circumstances for the passivity of stainless steels. It must be remembered that all the test solutions are far from the composition for an concentrated metal chloride solution inside a growing pit. Nevertheless, regardless of the initial bulk concentration, the final pit solution will always reach a high concentration if conditions are favorable for a stable pit growth (oxidizing conditions).

The ongoing rotating bending testing will show what effect the highly concentrated metal chloride solutions might have on the fatigue life length. It will be worth while to try to determine the critical pit depth from the fractured surface. The pit depth supposedly is in the range at least of 0.1 mm, and should be of detectable. By determining the pit growth rate and by determining of the threshold ΔK in the environment of interest, a calculation of the theoretical length of the incubation period is possible. The proposed mechanism can be validated by interrupting the wet period after different durations.

FUTURE PLANS

Continue near threshold fatigue testing of current test materials using an environment which simulates the composition of the electrolyte in a pit or crevice. Attempt to relate this data to cost per revolution at suction roll failure.

Complete the rotating bending fatigue testing of Alloys 63 and 75 in a simulated pit environment with concentrated ferrous, chromic, and nickel chlorides.

Investigate the effect of superimposed mean stresses on the crack initiation resistance of suction roll alloys in simulated white waters. This will to simulate residual stress effects.

FUNDAMENTALS OF DRYING

STATUS REPORT

FOR

PROJECT 3470

March 22, 1990

Institute of Paper Science and Technology
Atlanta, Georgia

PROJECT SUMMARY FORM

DATE: February 26, 1990

PROJECT: 3470 - FUNDAMENTALS OF DRYING

PROJECT LEADER: David Orloff

IPST GOAL:

Reduction of the "necessary minimum" complexity in number and/or sophistication of process steps.

OBJECTIVE:

To develop an understanding and a database sufficient for the commercialization of advanced water removal systems, based on high intensity drying principles. This new technology will reduce capital costs, increase machine productivity, reduce the amount of energy used, and improve properties.

CURRENT FISCAL BUDGET:

$150,000 from Institute funds, plus $300,000 through a Department of Energy grant (as Project 3595). This grant is for a total amount of $1.5 million over four years, this being the fifth of five budget periods for the project.

SUMMARY OF RESULTS FOR THIS REPORTING PERIOD:

(October 1989 - February 1990)

We have continued to concentrate our efforts on solving the delamination problem which is the major technical barrier to the commercialization of impulse drying. For background it is helpful to review some of our previous findings as summarized below.

- The probability of delamination at a given impulse drying process condition increases with increased ingoing sheet moisture. This effect has been explained by the fact that moist sheets absorb more energy from the platen and result in higher internal sheet temperatures. Coupling this effect with more available water, results in more energetic flash evaporation at nip opening.

- Pilot line trials have shown that use of a second impulse drying nip can heal sheet delamination caused by the first nip. These results have been confirmed using z-direction ultrasonic testing as well as by visual observation.

- Evaluation of a low thermal diffusivity ceramic platen showed that it significantly extended the range of impulse drying operating conditions without causing delamination. Although water removal was less than for steel, at similar operating conditions, ceramic platen temperatures could be increased to achieve equal water removal without inducing delamination. Heat flux measurements suggested that the ceramic platen was considerably more energy efficient than steel at similar amounts of water removal.

During the current reporting period our research program has consisted of four major elements; 1) comparison of ultrasonic and STFI compressive strength tests as means to quantify sheet delamination, 2) Validation of our heat flux measurement technique, 3) Verification of previous alternate platen experiments, 4) Determination of the effect of ceramic platen thermal diffusivity on platen performance.

COMPARISON OF ULTRASONIC AND STFI COMPRESSION TESTS:

Developing a method to quantify the extent of delamination of impulse dried specimens is of importance. Toward this objective we have previously reported the results of ultrasonic measurements of z- directional specific elastic modulus as compared to visual observation of delamination. When delamination was observed, the average value of the modulus decreases while the coefficient of variation of the modulus increases. In early work, Lavery used the STFI compression test to detect delamination. In the present reporting period we have completed a direct comparison of the z-direction specific elastic modulus to the STFI compressive strength index. Samples impulse dried with steel and ceramic platens, were tested at the same locations on each sheet by both tests. Figure 1 shows the correlation of the test results in which each data point represents a minimum of eight individual measurements. As expected, an increase in specific elastic modulus was also observed as an increase in STFI index.

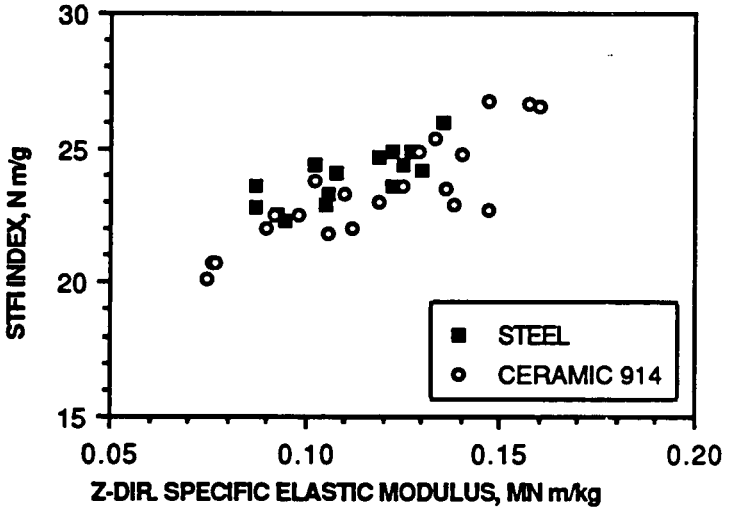

FIGURE 1. COMPARISON OF ULTRASONIC AND STFI TESTS

A comparison of the coefficients of variation of the measurements, is shown on Figure 2. Note that a large variability in modulus corresponds to a much smaller variability in index. Hence the modulus is expected to be a more sensitive measure of delamination.

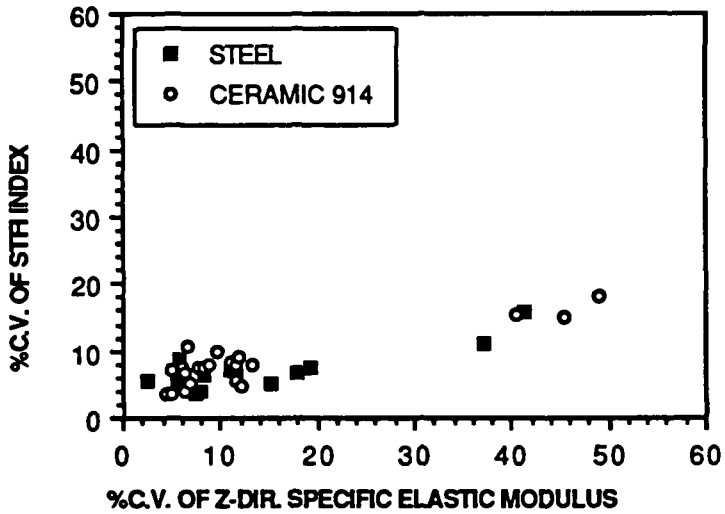

FIGURE 2. COMPARISON OF COEFFICIENTS OF VARIATION

VALIDATION OF THE HEAT FLUX MEASUREMENT TECHNIQUE:

In order to assess impulse drying energy efficiency we need to assure that heat flux can be accurately measured from both steel and ceramic platens. For this purpose, an experiment was designed to test the accuracy of the experimental heat flux measurement method compared to a heat transfer problem with a well known analytical solution. The experiment consisted of determining the heat flux when a heated platen of known temperature and thermal properties was quickly brought into contact with a cold platen of known temperature and thermal properties. In the experiments the surface thermocouples were located flush with the heated platen surface while and a thin conducting gel was used to eliminate contact resistance. Figure 3 shows the experimental settup.

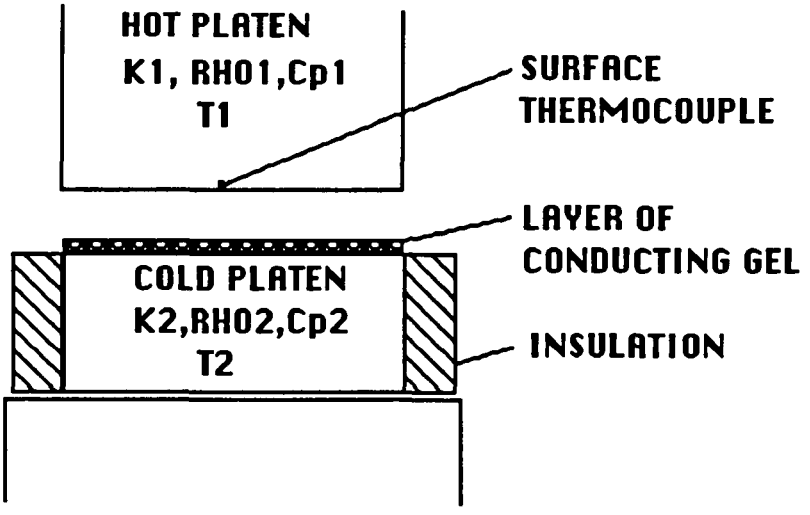

FIGURE 3. HEAT FLUX VERIFICATION EXPERIMENT

Comparison of heat flux results, shown in figures 4 and 5 indicate that except for the heat flux in the first few miliseconds, the experiment and theory were in excellent agreement. Hence, total energy transfer from the platens during impulse drying can be accurately measured. Note that, as expected, the heat flux from the steel platen was considerably higher than that for the ceramic platen.

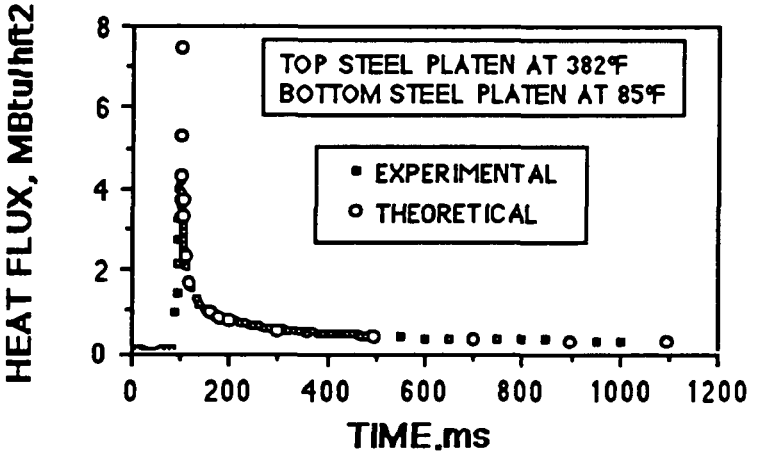

FIGURE 4. HEAT FLUX VERIFICATION FOR STEEL AGAINST STEEL

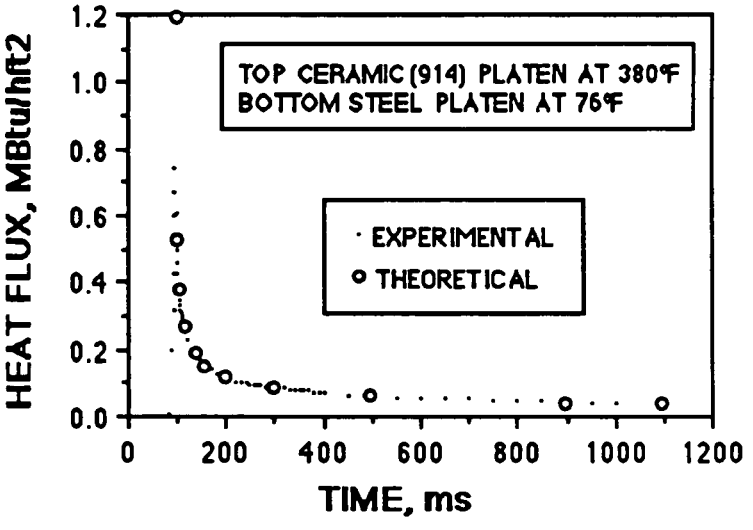

FIGURE 5. HEAT FLUX VERFICATION FOR CERAMIC #914 ON STEEL

VERIFICATION OF PREVIOUS EXPERIMENTS:

In our previously reported experiments, a machinable ceramic (Cotronic 914) platen was compared to a steel platen. Initial platen temperature and peak pressure were held constant while nip residence time was varied. Figure 6 shows a comparison of specific elastic modulus as a function of impulse for those experiments. The z-directional elastic modulus increases with increasing impulse as long as the sample does not delaminated. With an initial platen temperature of 260°C the steel platen caused delamination at an impulse of 32 psi s. At a similar initial platen temperature, the ceramic platen showed no signs of delamination up to an impulse of 38 psi s. With an increase in initial platen temperature to 315°C, the ceramic platen resisted causing delamination until an impulse of 55 psi s.

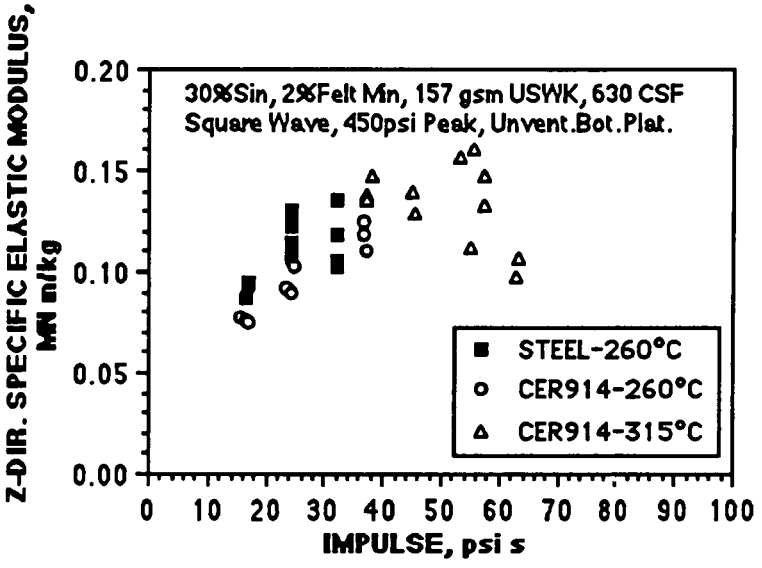

FIGURE 6. SPECIFIC ELASTIC MODULUS VS. IMPULSE

The extent of water removal, expressed as a moisture ratio change, was found to increase with impulse as shown on Figure 7.

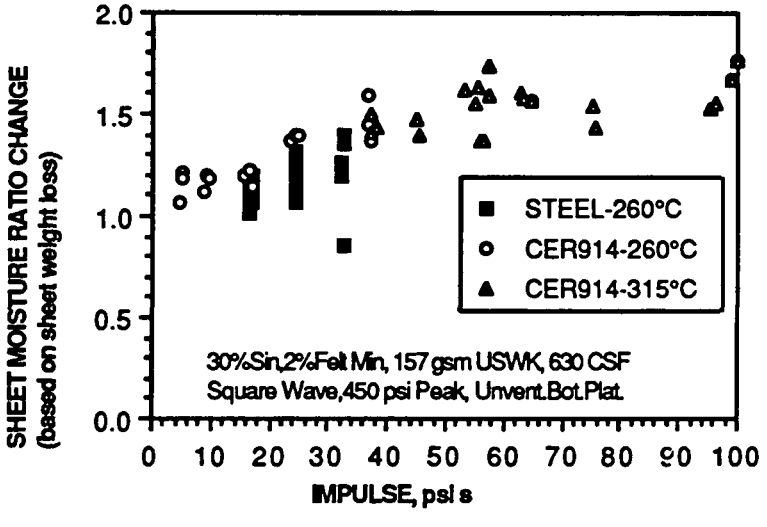

FIGURE 7. SHEET MOISTURE RATIO CHANGE VS. IMPULSE

We propose that platen performance can be assessed by determining the extent of delamination for a given amount of water removal. In Figure 8, the coefficient of variation of z- direction specific elastic modulus was used as a measure of delamination. A high variation occurs when an impulse dried sheet just begins to show delamination (ie some regions of the sheet are solid while others are delaminated). Referring to the figure, at an initial platen temperature of 260°C the steel platen caused delamination when the sheet moisture ratio change exceeded a value of 1.2. At the same initial platen temperature and sheet moisture ratio change, the ceramic platen showed no evidence of delamination. By raising the ceramic initial platen temperature to 315°C, sheet moisture ratio changes of 1.5 could be obtained without delamination.

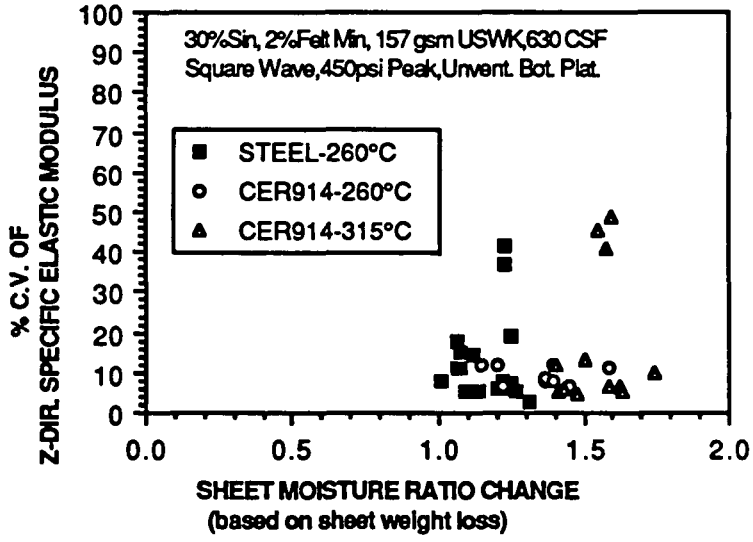

FIGURE 8. ALTERNATE PLATEN MATERIALS PERFORMANCE

These experiments clearly suggest that the ceramic impulse drying surface has distinct advantages over steel surfaces. In order to confirm that result, and to determine energy transfer with surface thermocouples mounted flush with the platen surface, a series of experiments were performed at various platen temperatures at constant impulse. Figures 9, 10 and 11 show the results of those experiments.

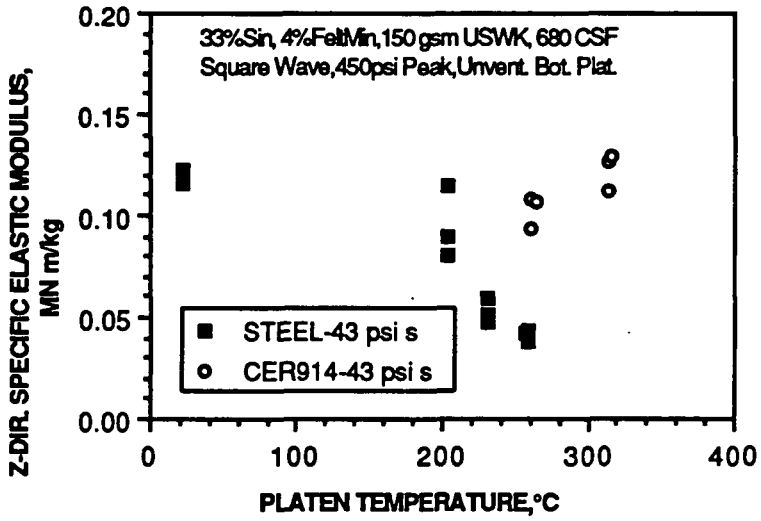

FIGURE 9. SPECIFIC ELASTIC MODULUS VS. PLATEN TEMPERATURE

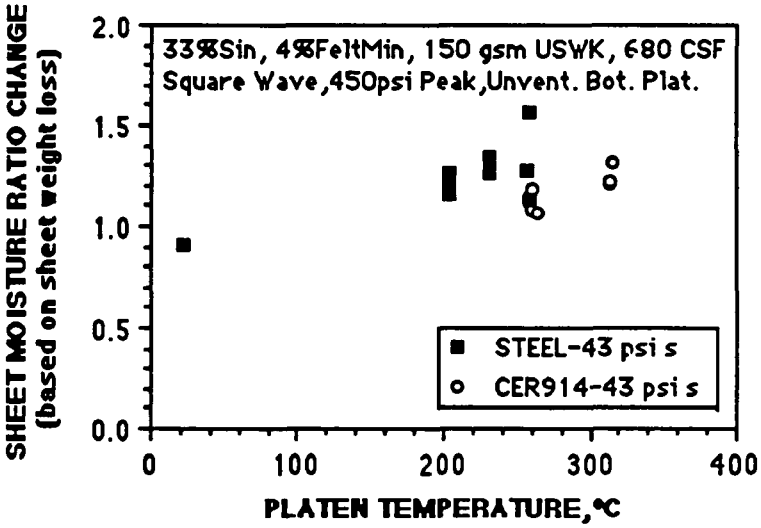

FIGURE 10. SHEET MOISTURE RATIO CHANGE VS. PLATEN TEMPERATURE

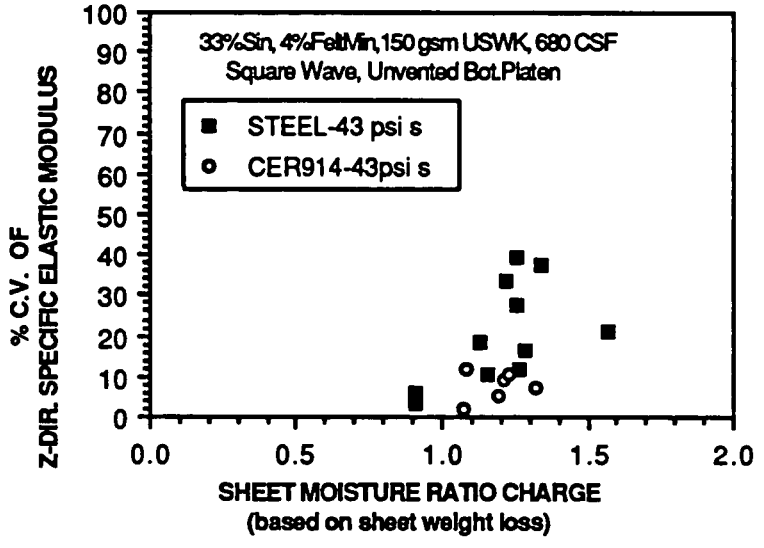

FIGURE 11. ALTERNATE PLATEN MATERIALS PERFORMANCE

Review of the figures shows that the steel platen resulted in delamination at 200°C while samples impulse dried using the ceramic platen showed no signs of delamination up to a platen temperature of 315°C. As in the previous experiments, the ceramic platen provided the same level of water removal but without delamination.

In previous experiments, the surface thermocouple was recessed into the platen surface in an attempt to prolong its useful life. In the current experiments care was taken to ensure that the surface thermocouples protruded from the surface (by not more than one mil). Surface temperature data along with known platen thermal properties were used to calculate the instantaneous heat flux and total energy transfer from the platen to the paper during the impulse drying event. Comparison of the results to those obtained previously indicated a considerable difference. Based on the latest data, previous energy measurements for the steel platen may have been underestimated by a factor of two, while previous energy measurements for the ceramic platen may have been overestimated by a factor of two. From the available information, it appears that precise location of the thermocouple at the platen surface is a prerequisite to accurate energy measurements. Future experiments, to precisely record energy transfer, will be designed such that the thermocouples location relative to the platen surface can be more accurately set.

THE EFFECT OF CERAMIC COATING THERMAL DIFFUSIVITY:

Because of advantages of manufacture, the ceramic impulse drying roll will be fabricated by plasma spray coating a ceramic onto a metal roll. In order to help define the thermal properties of that ceramic coating we have recently performed a series of experiments in which two different ceramic coatings were compared to the steel standard. The first coating, produced from aluminum oxide, was designed to have one tenth the thermal diffusivity of steel. The second coating, made from a mixture of zirconium oxide and yitrium oxide, was designed to have one hundredth the thermal diffusivity of steel. Both were plasma spray coated to a thickness of 17 mils onto a steel substrate and each was diamond ground to the same (40 rms) smoothness.

Ultimately a ceramic coated roll will be tested on the pilot (EHRID) dryer. In order to simulate the performance of the ceramic surfaces on the pilot dryer the shape of the pressure pulse was changed from a square wave to a haversine wave. In addition, the cold bottom platen was changed from an unvented to a vented geometry while felt initial moisture was raised to a level consistent with the design of the pilot dryer. In order to generate the same impulse as previous ceramic platen experiments, at similar dwell times, the peak pressure was raised from 450 psi to 900 psi. Table 1 shows a comparison of conditions.

TABLE 1. COMPARISON OF CONDITIONS

	PREVIOUS CERAMIC EXPERIMENTS	ALTERNATE CERAMIC COATING EXPERIMENTS
Felt % Moisture	2-4	16
Pressure Pulse Shape	Square	Havershine
Peak Pressure, psi	450	900
Cold Bottom Platen	Unvented	Vented
Basis Weight, GSM	150	200

The results of this most recent set of experiments are shown on Figures 12, 13 and 14.

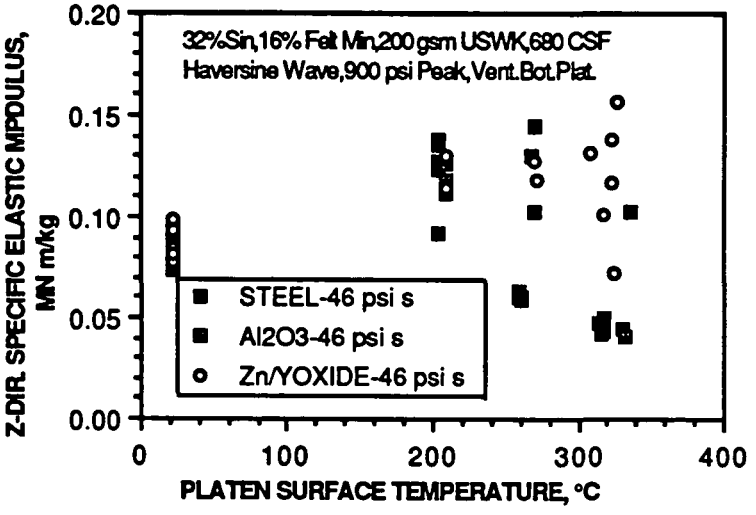

FIGURE 12. SPECIFIC ELASTIC MODULUS VS. PLATEN TEMPERATURE

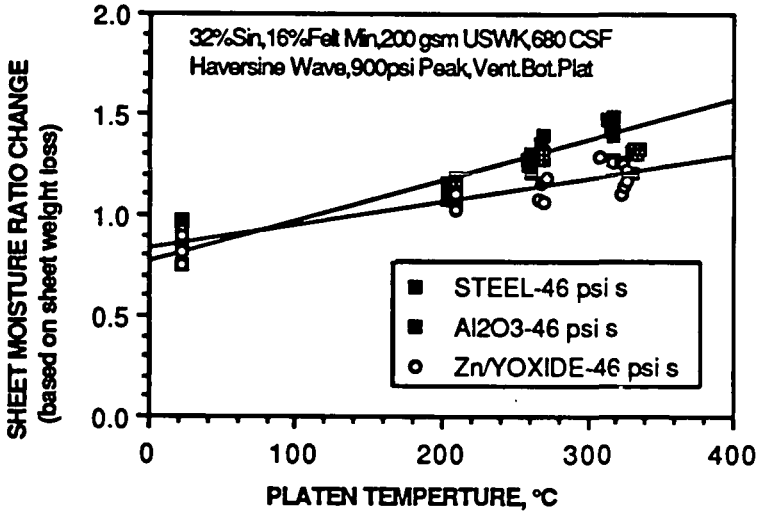

FIGURE 13. SHEET MOISTURE RATIO CHANGE VS. PLATEN TEMPERATURE

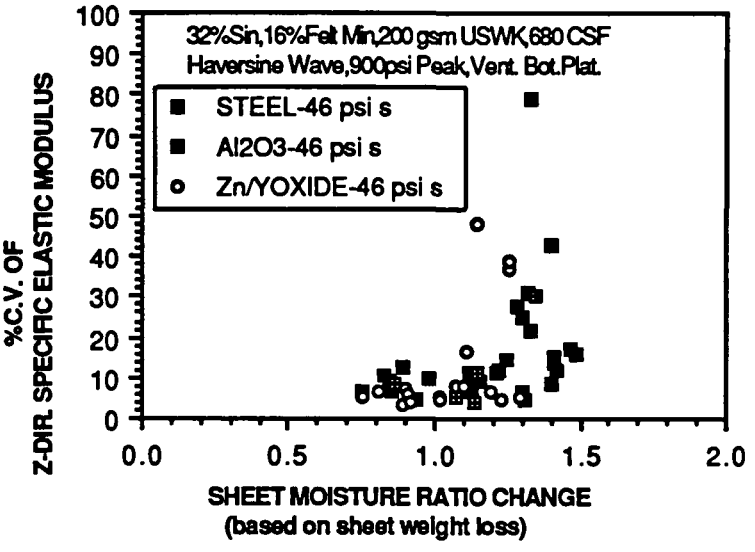

FIGURE 14. ALTERNATE PLATEN MATERIALS PERFORMANCE

Analysis of the data shows a result which is contrary to our previous findings. The steel and aluminum oxide platens performed similarly in terms of water removal and delamination, while the zirconium/yitrium oxide platen showed a lower level of performance. In future work we will resolve which of the modifications made in the most recent experiment caused the performance reversal.

PLANS FOR THE NEXT PERIOD:

Further work is planned in order to develop the ceramic roll surface concept. That work is expected to include the following tasks.

- Develop method for assuring that surface thermocouples are flush with the platen surface. Use surface temperature measurements to investigate the energy efficiency of alternate platen materials.

- Determine the reasons for the lower performance of the coated ceramic platens compared to previous experiments.

- Develop a master curve for impulse drying. The increase in moisture ratio will be correlated to impulse, total energy transfer and initial sheet energy for impulse drying. The results will also be compared to cold pressing at similar impulse and initial sheet energy.

- Design, fabricate and evaluate a ceramic coated roll on the pilot impulse dryer.

FUNDAMENTALS OF WATER REMOVAL PROCESSES

STATUS REPORT

FOR

PROJECT 3480

March 22, 1990

Institute of Paper Science and Technology
Atlanta, Georgia

PROJECT SUMMARY FORM

DATE: February 23, 1990

PROJECT NO.: 3480 – FUNDAMENTALS OF WATER REMOVAL PROCESSES

PROJECT LEADER: Jeffrey D. Lindsay

IPST GOAL:

Develop novel processes for efficient water removal with enhanced control over paper properties.

ABSTRACT

Several aspects of displacement processes are being explored to assist the development of impulse drying and to possibly develop new dewatering techniques. Impulse drying, which is considered a form of displacement dewatering because of the in-situ generation of a vapor phase, continues to present puzzles and challenges. The combination of numerical modeling and experimental work has not yet led to a full understanding of impulse drying physics. For example, improved heat transfer measurements now suggest that heat transfer is more intense than earlier measurements indicated, and this in turn implies that current numerical models are deficient in the handling of phase-change heat transfer. Recent fundamental work on boiling in model fibrous media has provided some basic information about boiling heat transfer, but this information cannot yet be safely applied to impulse drying.

Direct displacement dewatering, in which an injected gas phase drives water out of a mechanically compressed sheet of paper, has not yet been thoroughly tested. However, significant barriers to industrial implementation of direct displacement dewatering are evident. Further tests with the experimental displacement equipment will be possible soon, now that the MTS press is operational.

Of relevance to almost any water removal is the anisotropic permeability of paper, which controls two- or three-dimensional flows in paper. Such flows occur in press-nips and in displacement processes due to inherent instabilities at the gas-liquid interface. A new test program has been devised which will establish a database of anisotropic permeability information for a wide variety of papers. Full instrumentation for greatly improved measurements is nearly complete, and measurements will begin immediately.

New exploratory research has been initiated to exam the possible benefits of high-intensity ultrasound when applied to paper coating processes. In particular, the effect of ultrasound on dynamic particle-particle interactions near the blade in blade-coating will be explored, with the objective of improving runnability at high solids concentrations. Research-quality ultrasound equipment has been obtained, and preliminary experimental work in simple systems is underway.

REVIEW OF CURRENT PROJECTS

Vapor-liquid Displacement Processes

Impulse Drying Physics

Numerical Modeling

In order to better understand the physics of impulse drying, numerical models have been developed to predict the transient heat transfer, vapor pressure development, and vapor-liquid flow during an idealized impulse drying process. Recent efforts have focused on the role of a possible two-phase zone on impulse drying using predictions from MIPPS-II, a finite-difference computer model which solves the mass, momentum, and energy conservation equations for an idealized impulse drying-like process. MIPPS-II treats impulse drying as a one-dimensional process in which a vapor zone displaces a saturated liquid zone; a two-phase zone at equilibrium is allowed to form between the dry (vapor-filled) zone and the wet (saturated) zone, as shown in Figure 1. Details of the model were published recently in [1] and will not be given here.

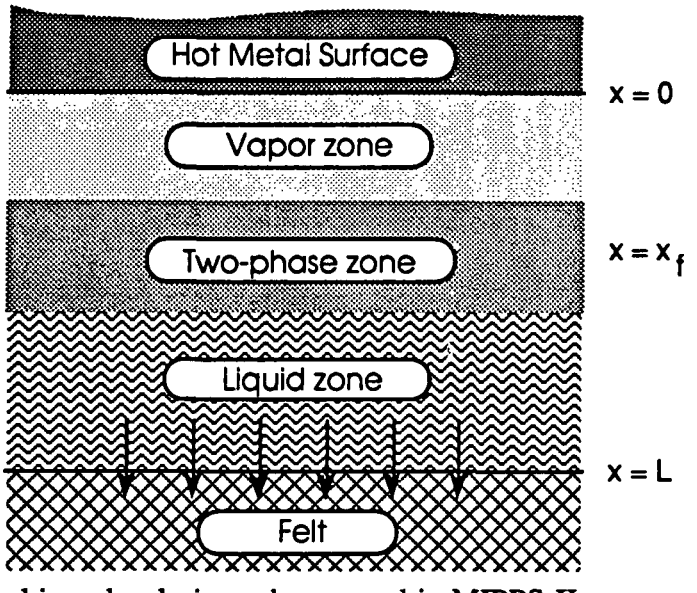

Figure 1. Idealized impulse drying scheme used in MIPPS-II.

Recently, new experimental data on heat flux in impulse drying has been obtained using improved instrumentation. Heat flux data are obtained from temperature measurements with a surface thermocouple in the hot platen of the MTS-based impulse-drying simulator. In previous

measurements [Lavery, Burton], the thermocouple was slightly recessed to reduce thermocouple damage; the effect of the recession on the heat flux data was assumed to be small. New measurements by Orloff with the thermocouple flush with the surface now indicate that previous heat flux data may have been low by as much as 50%. If this is indeed true, then MIPPS-II is unable to predict actual heat transfer rates without modifying the model to include significant capillary wicking effects, similar to the approach used in the earlier model, MIPPS-I. A proper treatment of capillary flow (a rigorous heat pipe mechanism) requires a substantial amount of experimental data which is not generally available for paper, but useful approximations may be possible.

In the last period, MIPPS-II was applied to more realistic cases than had been previously reported. In particular, previous predictions were made with sheets already near the boiling point; now predictions are being made with sheets initially at room temperature. This results in more severe thermal conditions which have frequently challenged the numerical approach of MIPPS, causing serious problems with convergence. Some cases still fail to converge; improving the numerics to handle all practical schemes is a current objective of the modeling work. A sample prediction of dynamic sheet temperatures at several locations is shown in Figure 2 for an impulse drying event with conditions and sheet properties applicable to current experimental work by Orloff. A linerboard sheet of basis weight 155 g/m^2 and initial solids content of 50% is used. The compressed sheet permeability is estimated to be 5×10^{-16} m^2 (reported sheet freeness is 620 CSF). The sheet is initially at room temperature (27°C). The sheet is impulse dried using a steel platen initially at 260°C (500°F). The transient temperature drop in the platen is predicted, which requires thermal properties of the steel.

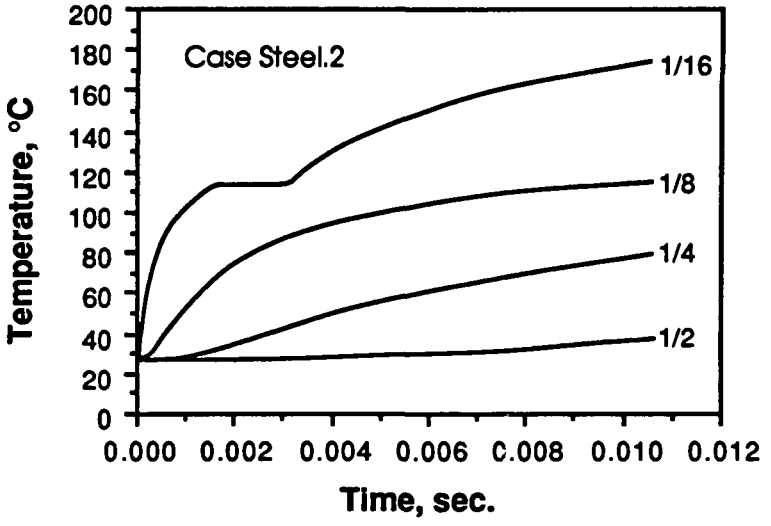

Figure 2. Prediction of local temperatures in a sheet during an impulse drying event. Sheet temperatures at depths of 1/16, 1/8, 1/4, and 1/2 the thickness of the sheet are shown.

The model has also been improved recently by incorporating a more accurate and more stable technique for predicting the temperatures in the heated platen or roll, which change because of heat transfer to the sheet. With this improvement, the effects of platen materials with different thermal properties can more easily be evaluated.

Efforts to include sheet deformation in MIPPS are underway. This project will ultimately require a rewrite of the model in convective coordinates, i.e., a transformed coordinate system which deforms with the paper. Such a transformation introduces a much higher degree of nonlinearity into the partial differential equations which must be solved.

Experimental Investigation of Boiling in Porous Media

In addition to numerical modeling, fundamental experimental work has been undertaken to elucidate some basic aspects of phase-change heat transfer in porous media. In particular, a heat transfer study of boiling in fibrous media has been conducted to gain insight into possible boiling mechanisms in impulse drying [2,3]. The results of this research are of fundamental importance in the field of boiling heat transfer.

Several pieces of evidence suggest that boiling may contribute to heat transfer during the impulse drying event. The occurrence of boiling within the fiber sheet in the short time frame of an impulse drying event presents a complex engineering problem. Understanding a model boiling process may provide insight regarding boiling heat transfer and the role of the vapor phase in impulse drying.

Experimental apparatus. Mechanistic studies of boiling phenomena begin with determination of the characteristic boiling curve, which is the relationship between heat flux and wall superheat (the difference between the heater surface temperature and the system saturation temperature). The experimental apparatus designed to gather data for boiling of water in a fibrous medium, illustrated in Figure 3, is discussed in detail elsewhere [4]. Briefly, the boiling cell apparatus is composed of four systems: the boiling cell, the heat supply system, the data acquisition system, and the process control system. The apparatus is designed to study heating block surface temperatures up to 400°C and cell pressures ranging from 0.10 to 0.28 MPa. The beds are composed of ceramic fibers with diameters of 3.0, 8.4, or 18.5 μm. Bed porosity ranges from 0.93 to 0.96, permeability ranges from 10^{-11} to 10^{-9} m^2, and average pore diameter ranges from 30 to 250 μm.

The boiling cell consists of a 9-cm ID x 110-cm long machined quartz cylinder. The fiber bed is formed in one end of the tube by filtration from a slurry having a consistency of approximately 0.1%. The tube is axially compressed between the heating block and a top mounting plate to seal the system for pressurized boiling.

The heating block, which is machined from a copper-tellurium alloy (ASTM B145), is 17.8 cm in length by 10.2 cm in diameter. Heat flow from nine cartridge heaters positioned symmetrically in a vertical orientation in the bottom of the heating block is metered by a silicon-controlled rectifier (SCR) based on the output signal from the surface temperature controller. Three thermocouples embedded within the block proximate to the boiling surface measure the temperatures necessary to calculate surface temperature and heat flux based on the one-dimensional heat diffusion equation incorporating a curve-fitted expression for temperature-dependent thermal conductivity of the block. An analog watt transducer measuring power supply to the cartridge heaters verified the accuracy of the technique for calculating heat flux.

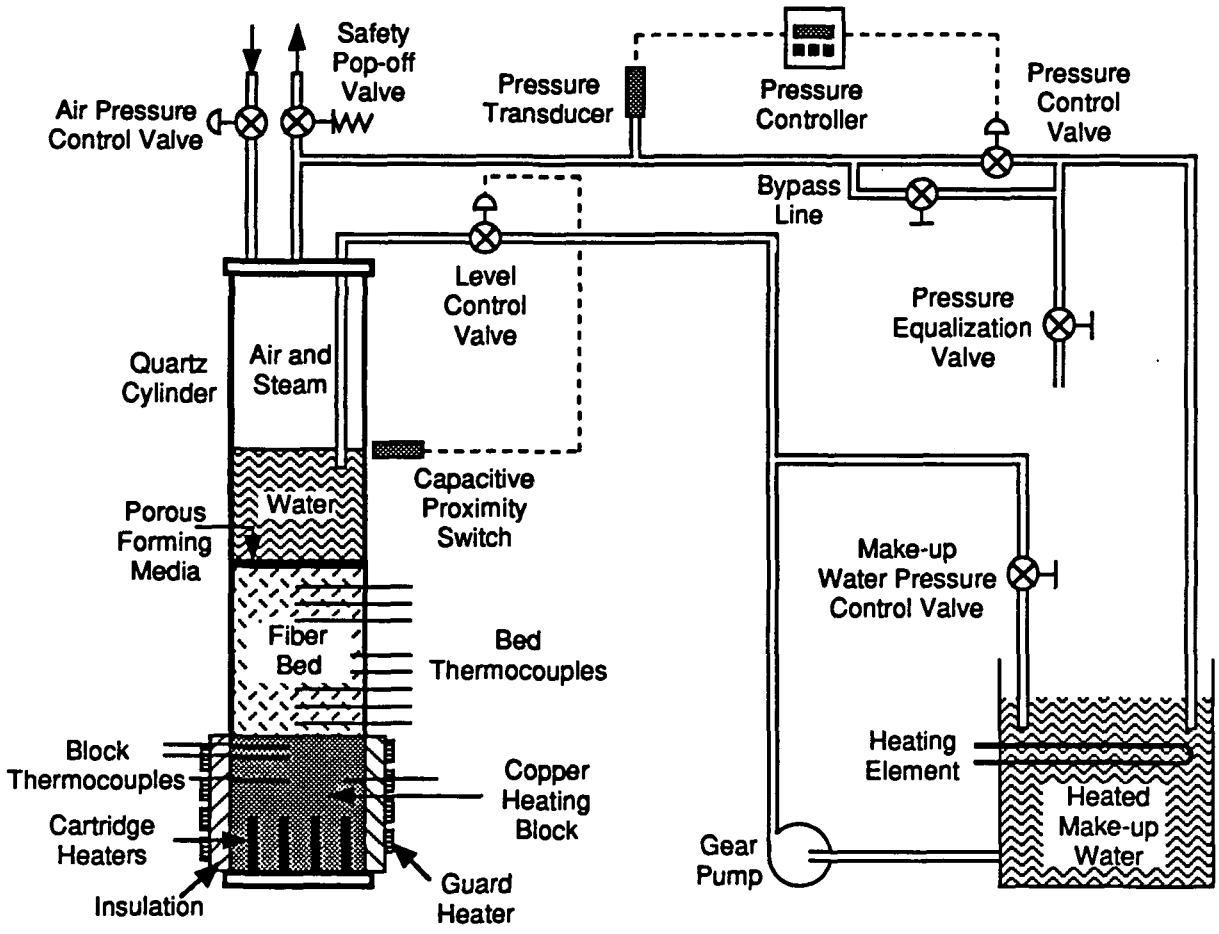

Figure 3. Schematic of the boiling cell apparatus.

The experimental control system developed for this apparatus provides data acquisition, heater block surface temperature control, and system pressure control. A number of type-K thermocouples and one strain-gage pressure transducer are interfaced with PID controllers and a computerized data acquisition system. Software was written to execute a steady-state boiling experiment.

Results from boiling experiments. Boiling experiments in fibrous media have been executed to determine the effects of medium pore diameter and system pressure on the characteristic boiling curve. Though the maximum pressure of 0.28 MPa used in this study is probably much lower than levels that develop within the cellulose fiber sheet during impulse drying, a catastrophic failure of the boiling cell at elevated temperatures at 0.28 MPa precluded boiling at higher pressures. The data comparisons to be presented are only intended to illustrate trends affected by experimental parameters. A more detailed discussion of the boiling phenomena are presented in References 9 and 11.

Once phase-change commences, vapor generated at the heater surface rises under the influence of a partial pressure gradient and buoyant forces, and liquid flows down to the heater surface under the influence of capillary forces and gravity. This two-phase zone of counterpercolating vapor and liquid is nearly isothermal, is at the saturation temperature for the system pressure, and grows in height with heat flux. The vapor condenses at the interface with the overlying liquid-saturated zone. If the height of this zone grows to encompass the entire bed, the vapor protrudes from the top of the bed and agitates the overlying pool of liquid. Fibrous beds with heights as high as 25 cm can become fully engulfed in two-phase flow.

Boiling is modified by the presence of the fibrous bed, as illustrated in Figure 4 (only the nucleate regime of the pool boiling curve for water is presented). The boiling curve for the fibrous bed exhibits two boiling regimes and a point of transition between them that represents the peak heat flux attained during the experiment. The direct dependence of heat flux on wall superheat in the initial regime is similar to the nucleate pool boiling regime. Heat transfer is limited by the ability of the heater to supply heat, which is related to nucleation characteristics of the heater surface. Apparently, some form of active nucleation is occurring at voids on the heater surface, within limits posed by physical constraints of the pore structure. Physical inhibition of nucleation may account for the reduced nucleate boiling effectiveness demonstrated with the

fibrous medium. It is during this nucleate-type regime that the isothermal, two-phase counterpercolation zone develops.

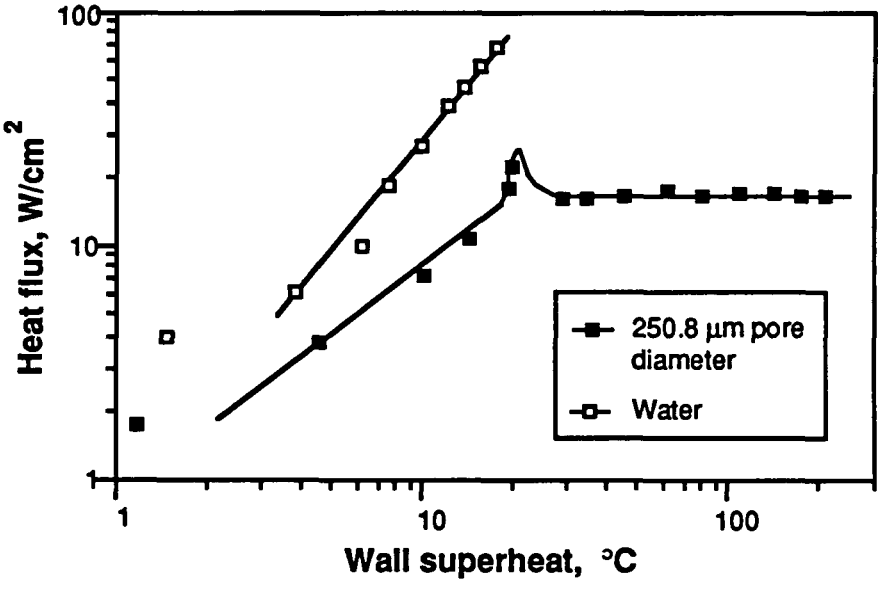

Figure 4. Typical measured boiling curves. Fiber diameter was 18.5 µm, porosity was 0.946, and permeability was 5.4×10^{-10} m^2.

In the second regime - called the constant-heat-flux regime, the heat flux is totally independent of wall superheat, as it is controlled by the rate of liquid flow to the heater surface under the influence of capillary forces of the bed. This obviously depends on the saturation level and pore size distribution of the bed. The point of transition between the two regimes, called the transitional heat flux (THF), can exhibit moderate instability. The beds with average pore diameters greater than 220 µm exhibit a peak heat flux that has a magnitude greater than that of the constant-heat-flux regime. At the THF, a dramatic change in the fluid flow phenomena reduces the heat-absorbing capacity of the bed. Attempts to increase surface temperature beyond the THF yield an instantaneous, rapid rise in surface temperature (typically, an increase of 10 to 15°C in a period of 10 to 15 seconds) until arrested by the surface temperature control system. The observed peak heat flux and subsequent decline to the constant-heat-flux regime for beds of large average pore diameter may be related to the saturation profile.

Effect of Average Pore Diameter. The average pore diameter of the bed significantly influences boiling phenomena, as illustrated in Figure 5. The slope of the nucleate-type regime decreases as pore diameter decreases, most probably because of the effects on the hydrodynamics of the vapor phase. Nucleation is probably inhibited, and the resistance to vapor flow away from the heater surface increases, in proportion to the diameters of the flow channels. Any accumulation of vapor at the surface will increase the resistance to heat transfer at the surface.

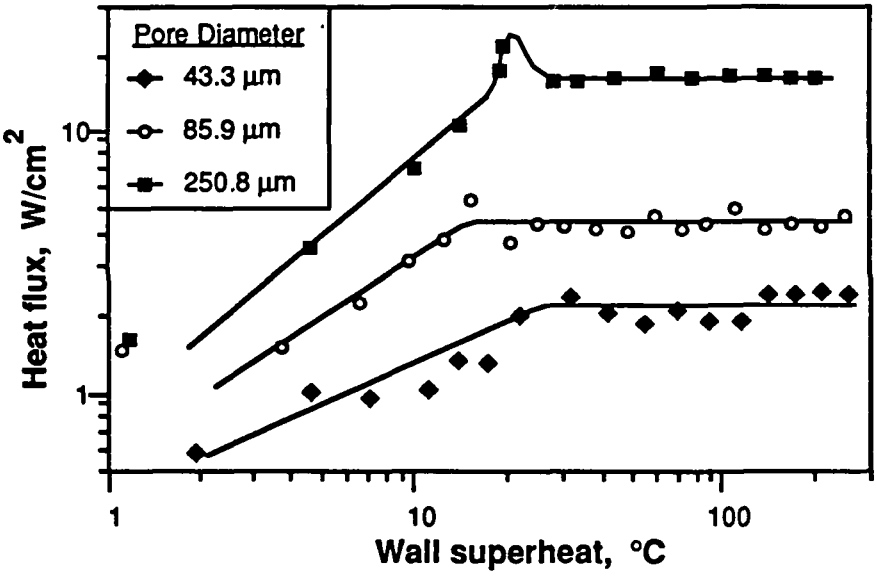

Figure 5. Effect of average pore diameter on the boiling curve at atmospheric pressure.

Behavior at the THF depends on the average pore diameter of the bed, as well. Each of the boiling curves for the large average-pore-diameter beds (220 to 260 μm) exhibits a distinct peak in heat flux between the two boiling regimes with an associated rapid escalation in surface temperature. However, the small average-pore-diameter beds (35 to 90 μm) exhibit a smooth transition. This difference in behavior at the THF may be related to the curvature of the saturation profile in the bed.

The magnitude of heat flux in the constant-heat-flux regime is directly related to average pore diameter. Obviously, as the pore diameters in a given type of porous medium decrease, the

permeability decreases, thus lowering the rate of liquid supply to the surface and also lowering the steady-state phase-change heat flux.

The Effect of System Pressure. Figure 6 illustrates the effect of system pressure on the boiling curves for fibrous beds with average pore diameters of approximately 250 μm. Prior to the region of transition, the nucleate-type regime is insensitive to pressure in the studied range. The effects of a higher bed saturation due to the increased vapor phase density at elevated pressures are not apparent in the heat flux data in the nucleate-type regime below wall superheats of about 20°C. This suggests that geometric constraints dominate pressure effects in controlling nucleation. The nucleate-type regime for beds with average pore diameters less than 90 μm also do not appear to be affected by pressure.

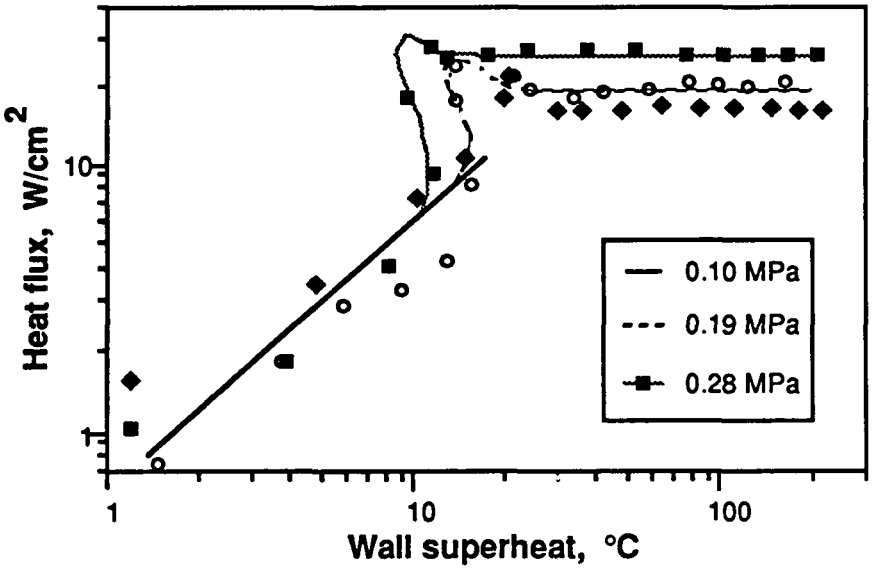

Figure 6. Effect of pressure on the boiling curve for a fibrous medium.

For beds with large average pore diameters, process instability at the THF is exacerbated as the system pressure increases. As the boiling process approaches the THF, the relationship between wall superheat and heat flux reverses, as the wall superheat actually decreases as higher heat fluxes are attained, exhibited as a backward bend in the boiling curve. Finally, the heat flux peaks and the surface temperature rapidly escalates. The behavior of decreasing wall superheat at increased levels of heat flux just prior to the transitional is reproduced in all of the pressurized boiling runs for beds with average pore diameters above about 220 μm.

The effect of pressure on the magnitude of heat flux in the constant-heat-flux regime is in part due to the increased density of the vapor phase. The consequent increase in bed saturation results in greater liquid water supply to the heater surface, which increases the heat-absorbing capacity of the bed. For all average pore diameters, the magnitude of heat flux in the constant-heat-flux regime is greater under pressure than at atmospheric conditions.

Implications for Impulse Drying. The highly porous model fibrous media and the steady-state experiments in this study will limit any application of the data to impulse drying. While the high peak heat fluxes observed early in impulse drying events clearly cannot be described in terms of the steady state boiling processes explored here, the fairly flat heat flux curves seen after about 20 msec in prolonged impulse drying may be approximated as steady boiling. Based on the results of this investigation, the latter portion of the extended impulse drying event may be controlled by an interaction of sheet pore size, pressure buildup within the sheet, and counterpercolation of steam and liquid water within the sheet. Gravity forces will be negligible, but capillary flow may be important, leading to a heat-pipe mechanism. In the constant-heat-flux regime, the characteristic curves for boiling in fibrous media demonstrate that heat flux is independent of thermal driving force, and depends on the pore size of the media and its ability to deliver liquid to the heater surface, and also on the system pressure. At this point, heat flux will be controlled by the rate at which the pore structure of the sheet can supply liquid water to the plane of evaporation for phase change. As with the model fibrous bed, a nearly isothermal zone, however thin, exhibiting counterpercolation of steam and liquid water delivers liquid to and vents vapor from the plane of evaporation. Thus, the heat flux will depend to a large degree on the pore structure of the sheet in this regime.

Conclusions. Boiling in the presence of a fibrous porous medium possessing significant capillary forces exhibits interesting phenomena that may provide insight into the role that boiling heat transfer plays in impulse drying. The average pore diameter of the bed and the system pressure are two factors that display a significant impact on both regimes encountered during boiling in a model fibrous medium. Consequently, the pore structure of the fiber sheet and the internal pressure that builds during impulse drying are expected to have a major impact on heat flux and the quantity of water removed during impulse drying. Based on this research, sheet pore diameter would seem to be the factor limiting the heat flux in the quasi-steady portion of an

extended impulse drying event, as the rate of water supply to absorb the heat at the interface of phase-change depends on pore size. The level of thermodynamic pressure within the sheet also controls heat flux due to its effect on sheet saturation.

Direct Displacement Dewatering

Direct displacement dewatering resembles impulse drying in that a pressurized gas phase assists in water removal. In direct displacement dewatering, however, the gas phase is added externally rather than being generated by heat transfer. Displacement dewatering differs from through drying in that the objective is to physically displace water rather than to evaporate it. It is thus critical that an effective water seal be established in the sheet, via compression, which can then be moved uniformly towards a felt by a gas phase. Such a process would permit water to be removed with less densification than is required by regular pressing, and with less energy than is required by evaporation. The objective is to provide the paper maker a greater degree of control over paper properties (bulk in particular), and also to yield an economically favorable process.

Experimental equipment to test the displacement dewatering concept was constructed prior to the move from Appleton, and is shown in Figure 7. Using an MTS electrohydraulic press, a sheet of paper is compressed between two drilled plates. A solenoid valve releases pressurized gas (air or steam) into the upper chamber, which acts to drive free water in the compressed sheet towards the underlying felt. The displacement dewatering apparatus requires the MTS press simulator, which, unfortunately, is in almost constant use for impulse drying studies. Only a brief series of preliminary measurement have been possible to date with the displacement dewatering apparatus. No new tests have been possible in the last period.

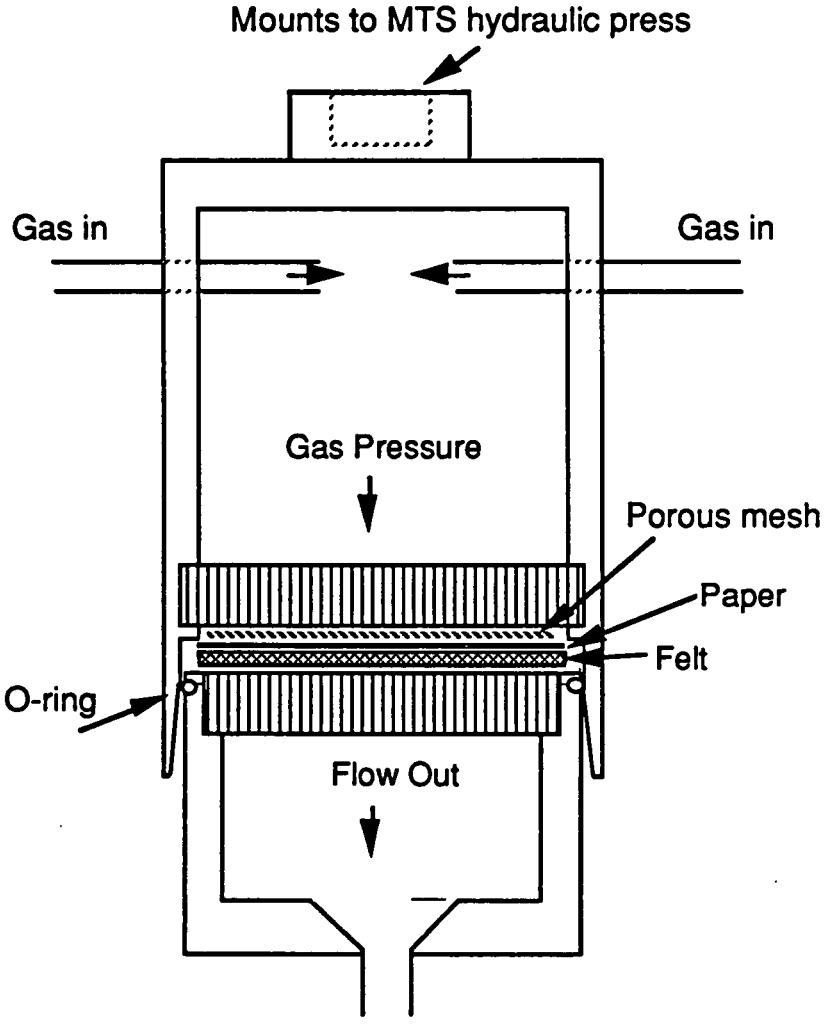

Figure 7. MTS press heads for displacement dewatering experiments.

The results from the only existing set of experiments with the current apparatus is shown in Figure 8. Compared to regular wet pressing, it does appear that displacement dewatering can give a higher degree of solid out for a given degree of densification, or higher bulk for a given solids out. However, several factors must be considered. First, a brief exposure to gas pressure does little good. At least 100 msec pressure pulse are required. Actual exposure to compressed gas was considerably longer in these runs, for although the MTS pressure pulse lasted 100 msec, the gas remained in the upper cylinder until it blew through the paper during the upstroke, in which the paper permeability was continually decreasing. Fairly simple computations, based on

the assumption of perfectly stable displacement, indicate that exposure to compressed gas at practical pressures must be sustained for on the order of 100 msec or longer to achieve a reasonable degree of dewatering. For example, consider the realistic case of a sheet which, when compressed at mild pressure, has a permeability of 2×10^{-16} m^2 and a thickness of 0.2 mm. Assume that gas at 100 psi is driving out the free liquid with perfect efficiency (no viscous fingering). The time required for the gas to move through 50% of the sheet is given by

$$t = \int_0^{0.5L} \frac{\mu}{K} \frac{(L-x)\,dx}{\Delta P} = \frac{3\mu L^2}{8 K \Delta P} = 0.108 \text{ sec}$$

Displacement dewatering may be most promising for highly permeable materials. We must also consider the formidable mechanical challenges of creating a high speed nip in which mechanical pressure and gas pressure can be simultaneously applied without significant leakage for approximately 100 msec.

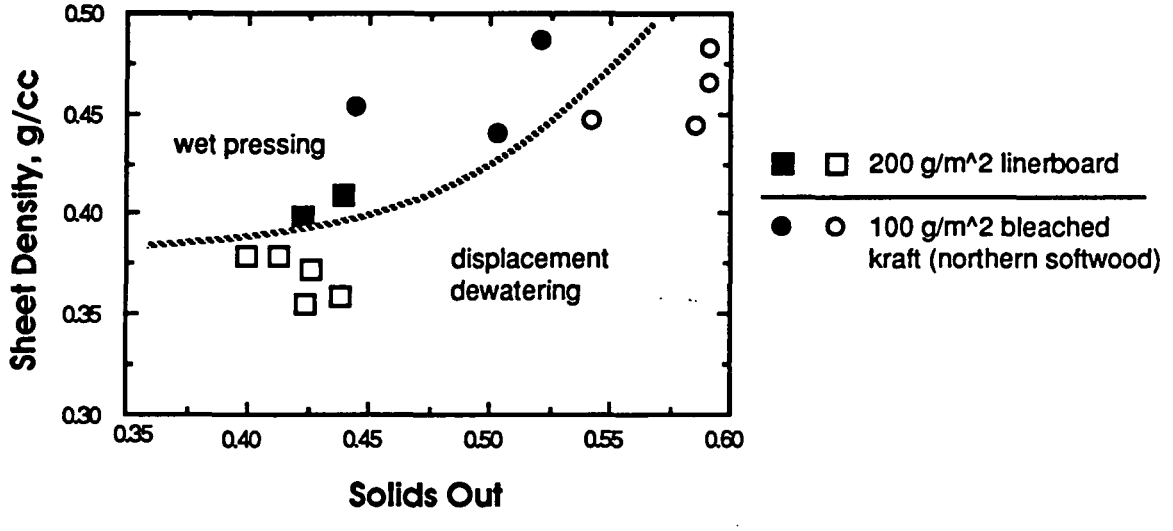

Figure 8. Sheet density versus solids out for wet pressing and displacement dewatering of handsheets.

Effects on Aqueous Suspensions

Standing ultrasonic waves can affect the orientation of non-spherical particles and fibers in suspension [7King, others]. For example, Brodeur et al. [8] have developed a technique for fiber analysis based on the effect of ultrasound on fiber orientation as a function of fiber properties.

F. Church reported in 1968 that ultrasound had a dramatic effect in promoting coagulation of fibers in paper stock. The effect indicated that changes in the electrical nature of the fibers had occurred [9]. More recently, Tarleton has reported that ultrasound and electric fields together can dramatically improve membrane filtration [10]. While electrofiltration has been investigated for some time, the role of ultrasound in filtration is less well understood, although the inertial and elastic forces generated by intense ultrasound are believed to modify the solid surface properties. Chemical, mechanical, and thermal effects may all play a role.

Possible Effects on Coating Color

There are a number of ultrasound effects which might assist a process such as blade coating. If ultrasound could be used to align clay platelets parallel to the sheet just before the color enters the gap, the flow behavior in the gap would probably be improved. Particle orientation in the gap is considered to be crucial, for the dimensions of clay particles, especially delaminated clay platelets, are on the order of the gap dimensions (ca. 10 μm diameter versus ca. 50 μm gap width), leading to the possibility of steric hindrance, unsteady clogging and dislodging, and other effects which would be manifest as poor runnability. The concept of ultrasonic assistance in blade coating is illustrated in Figure 9 below.

Ultrasonic Effects in Coating Application

Exploratory Research: Ultrasonics in Coating Application

Research has been initiated to explore the possible benefits of high-intensity ultrasound on the physics of coating application. The objective is to modify particle-particle or particle-blade interactions with external factors such as ultrasound in order to improve the runnability of the coating process. The results of work in other fields with ultrasound effects gives some reason to believe that ultrasound may have some potential in the area of paper coatings.

Background

Particle-particle interactions play a crucial role in determining the behavior of a coating color during application. Particle geometry, orientation, concentration, and electronic state all influence the flow behavior of the coating. As coating processes are driven to higher speeds, increased runnability problems are encountered which can be attributed to fluid mechanics instabilities. Delaminated clays, which offer high quality colors, pose particular problems. The high aspect ration of these particles lead to higher effective viscosities, and more runnability problems, at a given concentration than do other clays. The behavior of the color is largely controlled by particle-particle interactions, and also by particle-blade interactions in the gap in blade coating. If an external factor could be applied which would locally modify particle-particle interactions, improved control of the coating process may be possible. Ultrasound is now being considered for this role.

The Nature of High Intensity Ultrasound

A vibrating object in a fluid induces alternating compression and rarefaction waves. As high enough intensity, these waves can cause microbubbles to grow to and collapse. The result is shock waves in which local pressures can be hundreds of atmospheres, and local temperatures can exceed 3000°K. The intense mechanical and even chemical effects of sonication are sufficient to disrupt cells, disperse agglomerated solids, and emulsify liquids.

In addition to the mechanism of cavitation, the pressure generated by standing acoustic waves can affect particles and bubbles. The agglomeration of aerosols by ultrasound [6], for example, is a dramatic effect which led to the development of ultrasonic particle precipitators before the development of much less expensive electrostatic precipitators.

Effects on Aqueous Suspensions

Standing ultrasonic waves can affect the orientation of non-spherical particles and fibers in suspension [7King, others]. For example, Brodeur et al. [8] have developed a technique for fiber analysis based on the effect of ultrasound on fiber orientation as a function of fiber properties.

F. Church reported in 1968 that ultrasound had a dramatic effect in promoting coagulation of fibers in paper stock. The effect indicated that changes in the electrical nature of the fibers had occurred [9]. More recently, Tarleton has reported that ultrasound and electric fields together can dramatically improve membrane filtration [10]. While electrofiltration has been investigated for some time, the role of ultrasound in filtration is less well understood, although the inertial and elastic forces generated by intense ultrasound are believed to modify the solid surface properties. Chemical, mechanical, and thermal effects may all play a role.

Possible Effects on Coating Color

There are a number of ultrasound effects which might assist a process such as blade coating. If ultrasound could be used to align clay platelets parallel to the sheet just before the color enters the gap, the flow behavior in the gap would probably be improved. Particle orientation in the gap is considered to be crucial, for the dimensions of clay particles, especially delaminated clay platelets, are on the order of the gap dimensions (ca. 10 μm diameter versus ca. 50 μm gap width), leading to the possibility of steric hindrance, unsteady clogging and dislodging, and other effects which would be manifest as poor runnability. The concept of ultrasonic assistance in blade coating is illustrated in Figure 9 below.

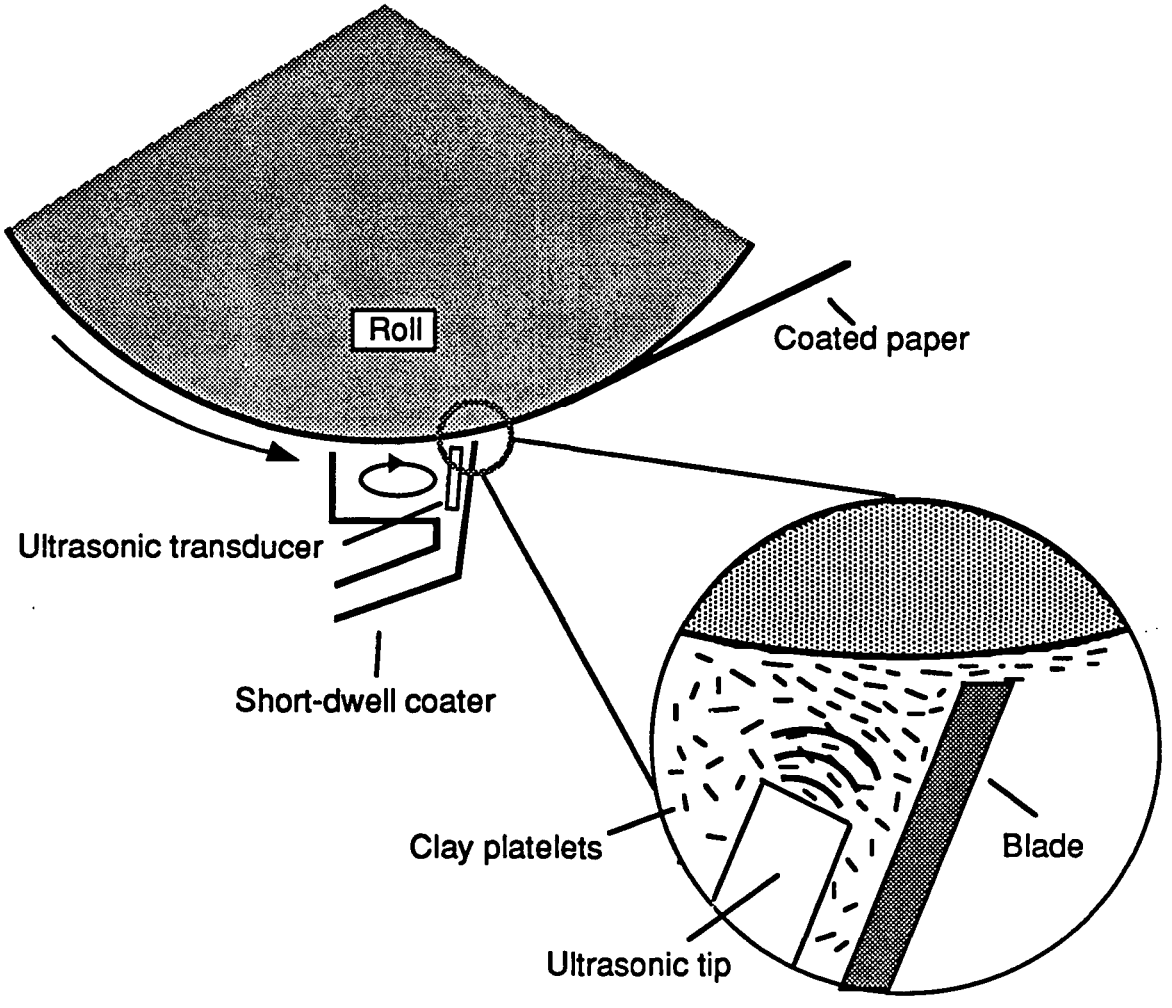

Figure 9. A possible implementation of ultrasound technology in a paper coating process.

Based on past research involving filtration, ultrasound may also lead to a favorable solids concentration gradient under the blade, with a high concentration next to the paper and a low concentration next to the blade being desirable. The question of exposure time becomes important: the brief exposure time at practical speeds may lead to no measurable effect, but then the dimensions of the necessary zone of application are also extremely small. Ultrasound is already used in several fields to improve the uniformity of slurries and to break agglomerates, but this effect requires long exposure times and would probably be of no significance in a coating

application process. Other roles of ultrasound have also been considered, but experimental work is needed to determine if there any beneficial effects are possible.

Experimental Approach

The experimental investigation of ultrasonic effects in paper coating will proceed in two stages. In the first stage, basic research will be done to determine the dynamic effect of ultrasound on suspension rheology, a topic which seems to have received little attention in the literature. Commercial coating colors and model suspensions will be investigated. Research-quality ultrasonic equipment with a continuous flow cell has been acquired from Heat Systems-Ultrasonics, Inc. The basic apparatus is shown in Figure 10 below. A high-intensity ultrasonic horn is held in a flow cell, which forces fluid through an orifice to flow across the tip of the horn.

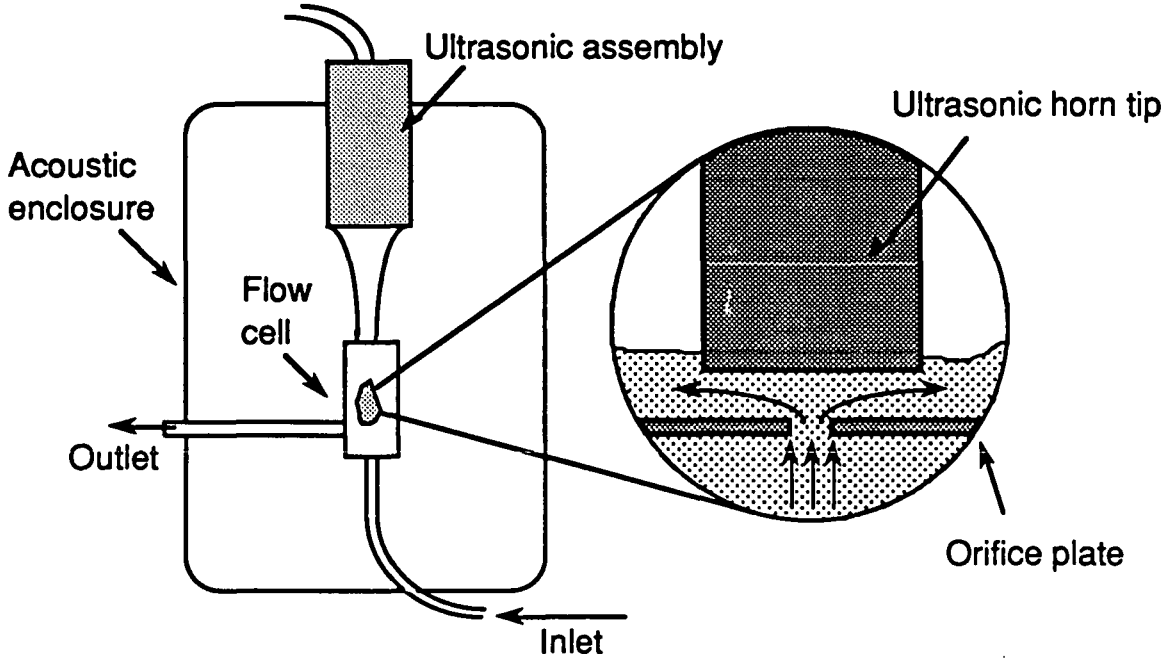

Figure 10. Ultrasonic horn and flow cell in acoustic enclosure. Power supply and wave generator are not shown.

The effect of ultrasound on flow behavior can be estimated by observing pressure drop across the orifice as a function of ultrasound intensity for a variety of flow rates and flow cell configurations. More fundamental data will be sought by inserting the ultrasonic horn into a capillary viscometer, near the capillary inlet, and measuring the change in apparent viscosity as a function of ultrasound strength. The IPST is currently deficient in viscometry equipment, but acquisition of a capillary viscometer suitable for coating color measurements is a current priority.

Following the rheological measurements, ultrasonic effects on coating application will be directly investigated using the IPST Keegan Coater and other pilot equipment.

Given the high capital and energy costs of high-intensity ultrasonic transducers, industrial application of ultrasound in coating – as currently envisioned – would be unfeasible for most grades. However, the advances made in exploratory research are rarely anticipated, and the new, fundamental information to be gained in this study may be valuable to the industry in unforeseen ways.

RECENT PUBLICATIONS AND PRESENTATIONS

Zavaglia, J. C. and Lindsay, J. D., "Flash X-ray Visualization of Multiphase Flow in Impulse Drying," Tappi J., 72(9): 79-85 (Sept. 1989); also presented at the 1989 TAPPI Engineering Conference, Atlanta, Georgia, Sept. 1989.

Lindsay, J. D., "The Physics of Impulse Drying: New Insights from Numerical Modeling," Fundamentals of Papermaking, Transactions of the Ninth Fundamental Research Symposium, Cambridge, England, ed. C. F. Baker and V. W. Punton, vol. 2, pp. 679-729, Mechanical Engineering Publications, London, 1989.

Lindsay, J. D., "The Anisotropic Permeability of Paper," 1989 TAPPI Engineering Conference, Atlanta, Georgia, Sept. 1989; accepted for publication in Tappi J. (1990).

Rudemiller, G. R. and Lindsay, J. D., "A Study of Boiling Heat Transfer in Porous Media," AIChE Annual Meeting, San Francisco, California, Nov. 1989.

Rudemiller, G. R. and Lindsay, J. D., "Apparatus for Investigating Boiling Phenomena in a Fibrous Porous Medium," Int. Commun. Heat Mass Transfer, 16(6): 785-794 (Nov./Dec. 1989).

Burns, J. R., Lindsay, J. D., and Conners, T. E., "Measurement of the Dynamic Behavior of Internal Sheet Structure During Wet Pressing," 1989 TAPPI Engineering Conference, Atlanta, Georgia, Sept. 1989; accepted for publication in Tappi J. (1990).

Burkhead, J. R., Lindsay, J. D., Burns, J. R., and Orloff, D. I., "The Effect of Felt Saturation and Other Felt Properties on Delamination in Impulse Drying," 1989 TAPPI Engineering Conference, Atlanta, Georgia, Sept. 1989.

Rudemiller, G. R. and Lindsay, J. D., "An Investigation of Boiling Heat Transfer in Fibrous Porous Media," accepted for The Ninth International Heat Transfer Conference, Jerusalem, July 1990.

Lindsay, J. D., "Advances in the Numerical Modeling of Impulse Drying," 1989 TAPPI Engineering Conference, Atlanta, Georgia, Sept. 1989.

PLANS FOR NEXT PERIOD

The main items planned for the coming period are:

1. Investigate the dynamic effect of ultrasound on slurry rheology. If possible, acquire a capillary viscometer.
2. Assist student research on anisotropic permeability.
3. Use the MTS press for displacement dewatering tests.
4. Continue refinement of MIPPS-II, including transformation to convective coordinates in order to model compression effects in impulse drying.

REFERENCES

1. Lindsay, J. D., "The Physics of Impulse Drying: New Insights from Numerical Modeling," Fundamentals of Papermaking, Transactions of the Ninth Fundamental Research Symposium, Cambridge, England, ed. C. F. Baker and V. W. Punton, vol. 2, pp. 679-729, Mechanical Engineering Publications, London (Sept. 1989).

2. Rudemiller, G. R., and Lindsay, J. D., "An Investigation of Boiling Heat Transfer in Fibrous Porous Media," accepted for The Ninth International Heat Transfer Conference, Jerusalem (July 1990).

3. Rudemiller, G. R., "A Fundamental Study of Boiling Heat Transfer Mechanisms Related to Impulse Drying," Doctoral Dissertation, Inst. Pap. Sci. Tech., Atlanta (July 1989).

4. Rudemiller, G. R. and Lindsay, J. D., "Apparatus for Investigating Boiling Phenomena in a Fibrous Porous Medium," Int. Commun. Heat Mass Transfer, 16(6): 785-794 (November/December 1989).

5. Lindsay, J. D., "The Anisotropic Permeability of Paper: Theory, Measurements, and Analytical Tools," IPC Technical Paper Series

#289, The Institute of Paper Chemistry, Appleton, Wisconsin (1988); accepted for publication in Tappi J. (1990).

6. St. Clair, H. W., "Agglomeration of Smoke, Fog,or Dust Particles by Sonic Waves," Ind. Eng. Chem., 41(11): 2434-2438 (1949).

7. Maidanik, G., "Torques Due to Acoustical Radiation Pressure," J. Acoustical Soc. Amer., 30(7): 620-623 (1958).

8. Brodeur, P., Dion, J. L., Garceau, J. J., Pelletier, G., and Massicotte, D., "Fiber Characterization in a Stationary Ultrasonic Field," IEEE Transactions on Ultrasonics, Ferroelectrics, and Frequency Control, 36(5): 549-553 (1989).

9. Church, F., "A New Approach to Filtration," Symp. Consistency Measurement and Control, 1968.

10. Tarleton, E. S., "How Electric and Ultrasonic Fields Assist Membrane Filtration," Filtration and Separation, 25(6): 402-406 (Nov./Dec. 1988).

RECOVERY BOILER FIRESIDE CORROSION

STATUS REPORT

FOR

PROJECT 3628

March 22, 1990

Institute of Paper Science and Technology
Atlanta, Georgia

PROJECT SUMMARY FORM

DATE: March, 5,1990

PROJECT: 3628 - Recovery Boiler Fireside Corrosion

PROJECT LEADER: Per-Erik Ahlers

IPST GOAL:
Improve safety and increase the operating life of equipment by proper selection of construction materials and by identifying suitable process conditions.

OBJECTIVE:
To understand the causes of corrosion on the water wall tubes in the lower part of kraft recovery boilers on the:

1) furnace side (hot side), and
2) wind box side (cold side),

as a basis for devising methods of reducing corrosion damage.

CURRENT FISCAL BUDGET: $160,000.

PRIOR RESULTS:

Laboratory results related to hot-side corrosion.

The test environment containing smelt powder and nitrogen gas caused only mild corrosion on carbon steel (0 - 2 mpy) in two week exposures at 300 and 400°C. In the short term runs (5 hours) without smelt powder, an aggressive test gas containing H_2S and O_2 did not cause corrosion on stainless steel even at 400°C. However, the presence of smelt powder activated the corrosion, and corrosion rates around 20 and 60 mpy were measured at 300°C and 400°C. For carbon steel the corresponding figures became 15 and 100 mpy with the gas alone, and 200 and 350 mpy with smelt powder present. Thus, the synthetic smelt powder in contact with

the metal aggravated the corrosion conditions significantly. Elemental carbon in contact with the metals had no additional effect. The gas flow rate in the tube furnace between 0.15 - 0.45 m/hr (3 - 9 l/h) was found to be noncritical. One of the key conclusions in the Ph. D. thesis by Greg Kulas was that the relatively high corrosion rates encountered in mill practice (0.5 - 1.5 mm/yr) are possible if the metal is periodically exposed every 12 hours for a very short time period to the aggressive lower furnace gas. Otherwise the rate will be at least on decade lower.

Laboratory Results Related Cold-side Corrosion

Potentiodynamic curves obtained in a sodium hydroxide melt at 320°C indicated that introduction of water vapor into the gas phase over the melt increases corrosion of both carbon steel and stainless steel. The initial free corrosion potentials were all within the passive region.

Field Testing

Two access ports were installed in a B&W boiler for the cold side corrosion trials. Two corrosion probes were redesigned and constructed. The design of a hot side probe is underway.

SUMMARY OF RESULTS SINCE LAST REPORT

The experimental work has been delayed due to factors related to relocation, the new working environment, and under-staffing. However, we have reviewed our understanding of the important factors in boiler corrosion. In this review some thoughts were raised about reaction mechanisms leading to the high corrosion rates observed in service and how studies should be directed to clarify if gas formation is associated with the phenomenon.

Polarization curves obtained in molten sodium hydroxide have exhibited satisfactory repeatability. Moreover, they have shown that addition of 10 wt.-% sodium chloride spontaneously activates the carbon steel surface which otherwise remains passive in pure hydroxide melt. The presence of chloride in the hydroxide melt induces only minor changes in the electrochemical behavior of carbon steel and stainless steel. The passive current density is slightly increased and the active peak current depressed by chloride. Corrosion rates corresponding to the measured anodic currents were in general extremely high. In the active range the peak rates for carbon steel were around 50,000 mpy and the corresponding figure was one decade lower for stainless steel.

FUTURE WORK

Laboratory experiments will continue and field testing will be initiated related to hot and cold-side corrosion. Based on thermodynamic calculations, potential gas generation reactions will be studied.

RECOVERY BOILER FIRE-SIDE CORROSION
Project 3628

REVIEW OF KEY FACTORS IN FIRE-SIDE CORROSION

The question about which factors control the corrosion process on the fire side of water wall carbon steel tubes in the lower part of recovery boiler furnaces is still partly open. Some of the contributing factors are well known, but which of these is the rate governing stage in the corrosion process is still unclear. Laboratory tests have given extremely high corrosion rates when carbon steel is exposed to gas or gas/smelt powder for a short time period, and very low rates when the specimens are covered by a frozen smelt layer when immersed into a smelt pool. By realizing that the water wall tubes are normally covered by a relative thick smelt layer (approximately one inch thick) it is difficult to understand how the highest corrosion rates seen in practice are possible.

The gas in the lower furnace is corrosive toward bare carbon steel and extremely high corrosion rates (18.8 mm/yr) have been measured in short term laboratory experiments (Dahl, L. and Falk, I.; Investigation of Alloyed Steels for use in Black Liquor Recovery Boilers - Report 3, Swedish Corrosion Institute, Stockholm, Sweden (1972)). The gas is most aggressive when it initially consists of roughly equal amount of H_2S and O_2 plus reducing gases, i.e., the presence of H_2 and/or CO. In fact, the most aggressive corrosion conditions in the boilers exists in the neighborhood of primary and secondary airports where oxygen in the combustion air is consumed down to a level of that of H_2S in the gas phase (around 0.1 %).

In exposing carbon steel to a gas containing either H_2S or O_2, the corrosion rate will be considerable lower than with a mixture of the two. Hydrogen sulfide and oxygen react easily with each other forming elemental sulphur and SO_2 plus water as a by-product. Both of the sulphur species are reactive toward carbon steel. With sulphur alone the corrosion products will be poorly protecting iron sulfides. The SO_2 partly dissociates at a high temperature to sulphur and oxygen. Depending on the conditions (temp., pO_2) the reaction products could be either sulfides or oxides or a mixture of both. Under reducing furnace

conditions the oxygen in the SO_2 is consumed by H_2 or CO, and the remaining sulphur will react with iron and forms sulfides.

A frozen smelt layer covering the tubes lowers the corrosion rate significantly. However, Dahl and Falk found in their experiments that with a thin smelt layer (1 mm) the initially low corrosion rate increases remarkably after 4 hours exposure at 400 ^oC under aggressive gas atmosphere (Investigation of Alloyed Steels for use in Black Liquor Recovery Boilers - Report 4, Swedish Corrosion Institute, Stockholm, Sweden (1972)). The reason for this radical change is unclear. The composition of the "aged" smelt was slightly changed in a way that indicates both the sulphur and SO_2 in the gas phase could have reacted with the metal covering smelt, i.e., the polysulfide and the sulfite content where higher and the carbonate content was lower.

The main conclusion made by Greg Kulas in his Ph.D thesis , "AN INVESTIGATION OF SOME FACTORS AFFECTING THE CORROSION OF CARBON STEEL BOILER TUBE MATERIAL EXPOSED TO SIMULATED KRAFT SMELT", IPST, 1989, was that the high corrosion rates (0.5 - 1.5 mm/yr) observed in service are an impossibility if a stationary smelt layer covers the metal surface with an underlaying corrosion scale. The scale seems to control the corrosion rate, but if the metal is periodically exposed to the aggressive boiler gas even for very short time periods an average corrosion rate in an magnitude of 1 mm/yr could be maintained. It is unclear what forces could be responsible for a potential process that rips off the smelt layer and adherent corrosion products. The top coat of the smelt layer is continuously renewed by the down flowing smelt film on top of the frozen layer and is therefore stabilized. Below the molten surface, at the reaction sites close to the metal, reactions take place resulting in slow changes. Stresses in the corrosion layer are built up, decreasing the adhesion between the corrosion products and the metal. Gas forming reactions would contribute to push off the smelt layer and adherent corrosion products making the conditions more conducive to higher corrosion rates. For instance, in reactions of carbonate with polysulfide, sulphur, or thiosulfate, CO_2 and/or CO is produced.

Corrosion tests conducted at IPST with metal coupons have shown that the presence of smelt powder makes the corrosion conditions significantly more severe. The most likely reason for that is that the acidic components in the test gas, CO_2 and H_2O, might react with

sodium sulfide giving rise to a partial sulphur pressure in the gas phase thus enhancing the corrosion.

On the cold side of the water wall tubes, corrosion attack has been experienced on composite tubes. It is believed that a liquid phase is fluxing the protective passive layer from the stainless steel surface. One possible explanation is that sodium hydroxide vapor is diffusing from the furnace gas space through openings in the water wall and condensing on the cooler back side of the tubes. Narrow cavities are preferential locations for condensation because the pressure inside the gap is lowered due to surface effects, and such cavities have appeared to be also preferential locations for corrosion attacks.

Stainless steel is more susceptible to corrosion than carbon steel when exposed to molten hydroxide, especially under oxidizing conditions. In practice it has been experienced that even the corrosion rate is higher for stainless steel than for carbon steel. A. Rahmel et.al. studied the solubility of iron oxides and chromium oxide in hydroxide melt under different gas atmospheres. They found that water vapor retards and oxygen accelerates the solubility of chromium oxide in the melt and the reaction rate (A. Rahmel and W. Schwenk; Korrosion und Korrosionsschutz von Stählen, Verlag Chemie, New York, 1977, p. 304)

Based on the polarization curves measured at IPST it was concluded that water vapor in the gas over a NaOH melt increases the corrosion rate with the metal in an active or passive state both for the grade 304 stainless steel and for carbon steel (Status report for Engineering Project Advisory Committee, October, 1989). This result seems to be in contradiction with Ramel's results and has to be checked.

LABORATORY EXPERIMENTS AT IPST

A) Coupon Tests

Several difficulties were encountered in initiating the coupon tests in Atlanta. These included lack of installed 220 V electricity in the corrosion lab, problems with the delivery of special gas mixtures, broken furnace tubing, and a delay in getting the grit blaster in service. By the time of the PAC meeting, all these obstacles will be eliminated and the experiments underway.

B) Sodium Hydroxide Melt Experiments

The polarization curves are measured using an improved electrode holder. Previously it was observed that the ceramic cement used in Appleton to seal the metal electrodes to the alumina tubing was not completely inert in the molten NaOH environment and had to be renewed frequently. This cement was based on MgO powder. The new one is composed of Al_2O_3 and seems to be much more resistant.

The first polarization curves obtained in NaOH melt under pure N_2 gas in Atlanta are similar to the previous curves, and consequently the cement has not interfered with the results. The results show the carbon steel exhibits higher corrosion rates than stainless steel within both the active and passive region. The free corrosion potential in both cases was located inside the passive region.

Figures 1 and 2 show examples of polarization curves and the degree of reproducibility of the data obtained under a dry, nitrogen atmosphere. From the graphs it is evident that the repeatability is relatively good. The reference electrode used is not entirely stable and therefore the curves could be shifted slightly sideways. Regarding the results for stainless steel, the size of the active peak seems to depend on how well the surface is initially activated, which also indicates that the environment is not very harsh toward stainless steel. However, with the electrode surface area being only 0.3 cm^2, the seemingly low current data represents relatively high corrosion rates. At a current level of 1 mA the corrosion rate corresponds approximately to 30 mm/yr (1200 mpy).

Introducing 10 % NaCl into the hydroxide melt activates the carbon steel which otherwise remains passive in pure hydroxide melt under reducing test conditions (Fig. 5). The presence of chloride in the hydroxide melt induces only minor changes in the electrochemical behavior of carbon steel and stainless steel. The passive current density is slightly increased and the active peak current depressed by chloride (Figs. 5 and 6).

The free corrosion potential, determined before every run, appeared to be in all cases within the passive region, i.e., on the right hand side of the active peak, with an exception of carbon steel in hydroxides doped with chloride (Fig. 3). The active peaks for carbon steel are considerable higher than that for stainless steel indicating a greater risk for corrosion. So far all runs were conducted under reducing conditions, and the next step is tests under oxidative condition.

FUTURE PLANS

The purpose of the cold-side field experiments is to learn what kind of deposits are condensing in a real situation at different temperatures on a stainless steel surface. Besides this, corrosion rate monitoring and trials to measure the electrical conductivity in the deposit will be employed. Supplementary electrochemical laboratory experiments will be performed which are expected to support the field findings. The target with the hot-side field experiments is to collect genuine corrosion-smelt layer products to analyze the composition of corrosion product-smelt layer from different conditions in order to find out what mechanism is responsible for the high corrosion rate.

The investigation of the effect of several inorganic chemicals such as thiosulfate, sulphur, sulfite, and chloride added to the smelt powder mixture will continue according to plans made earlier. In order to investigate chemical and electrochemical reactions with gas evolution thermodynamic calculations will be made. The electrochemical experiments in hydroxide melt will continue to clarify the role of water vapor, CO_2, and O_2 on corrosion in molten phase. The field work will be initiated to investigate the cold side corrosion in recovery boilers. The probe for hot side corrosion experiments will be constructed and bench tested.

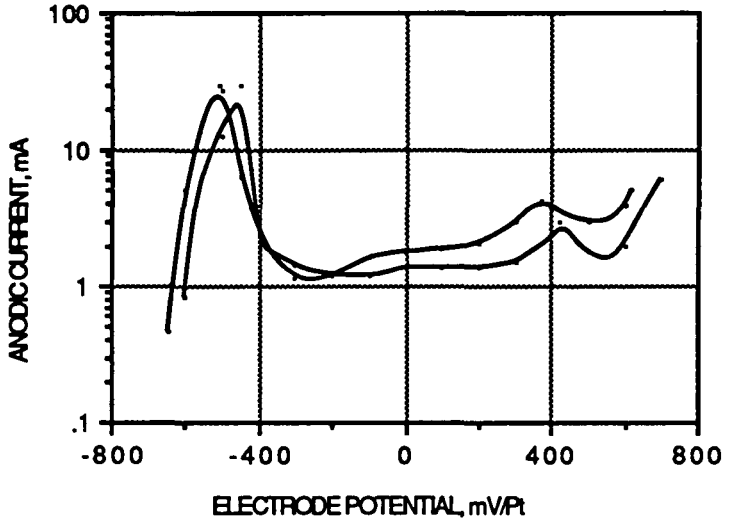

Figure 1. Comparison of two polarization curves for carbon steel obtained under similar conditions in NaOH melt containing10 % NaCl.

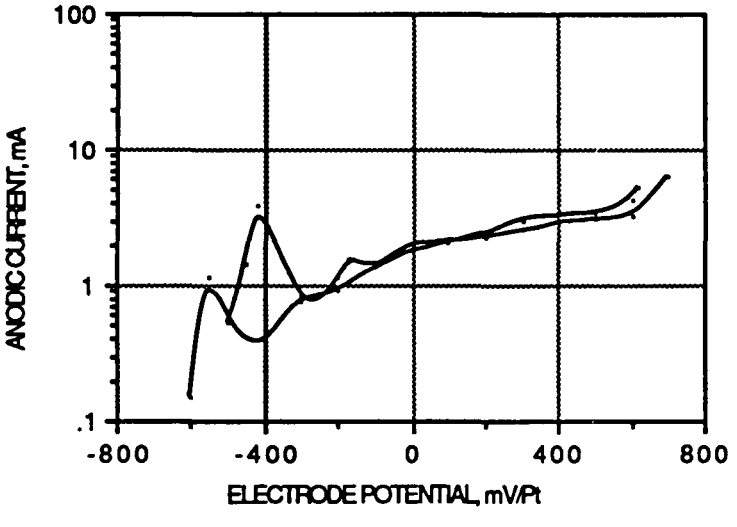

Figure 2. Comparison of two polarization curves for stainless steel (304) obtained under similar conditions in NaOH melt containing10 % NaCl.

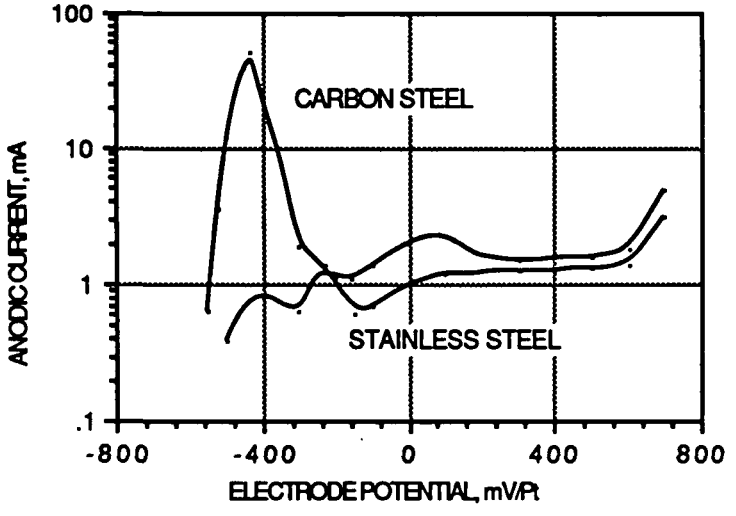

Figure 3. Polarization curves for carbon steel and stainless steel obtained in chloride free NaOH melt under N_2 at 320 °C. Surface area=0.3 cm^2.

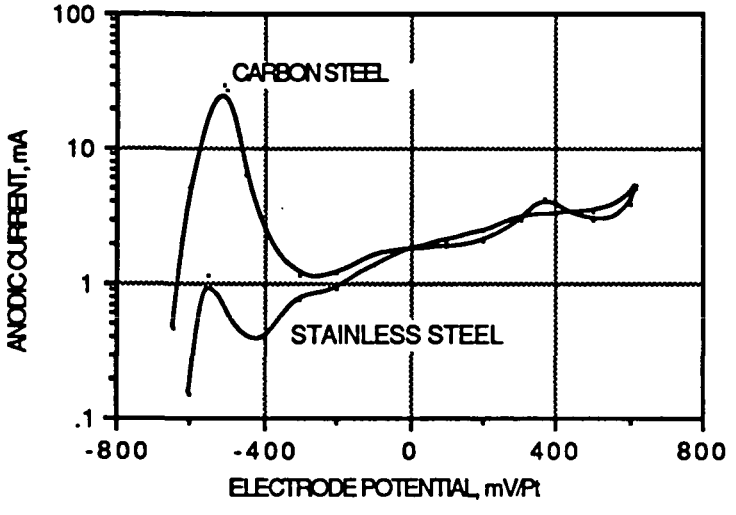

Figure 4. Polarization curves for carbon steel and stainless steel obtained under N_2 at 320°C in NaOH melt containing 10% NaCl. Surface area=0.3 cm^2.

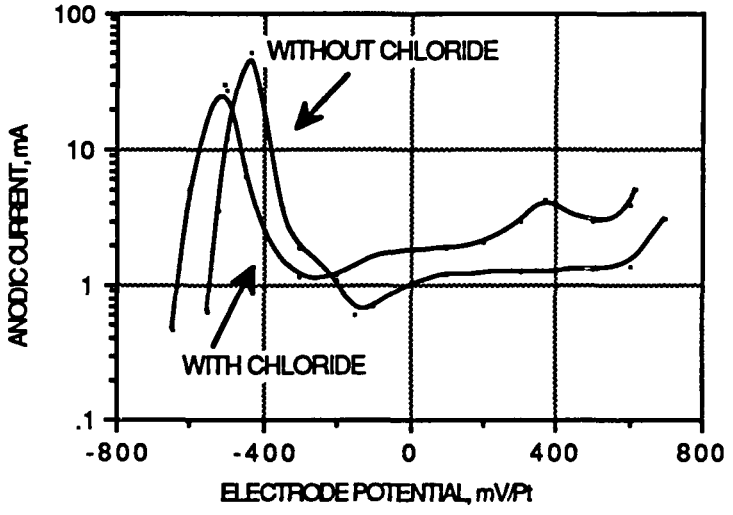

Figure 5. The effect of chloride (10%) on polarization curves obtained in molten NaOH at 320°C for carbon steel with a surface area of 0.3 cm^2. The initial free corrosion potential was in the passive range (E=407 mV), but in chloride doped hydroxide active(E=505 mV).

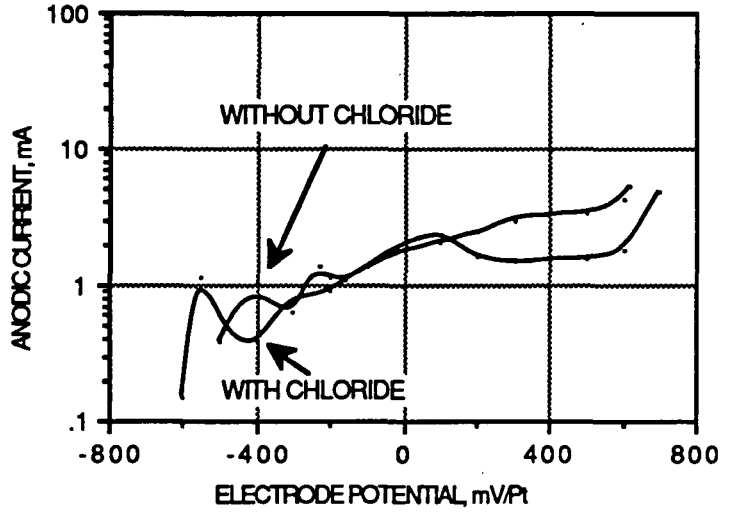

Figure 6. The effect of chloride (10%) on polarization curves for stainless steel with a surface area of 0.3 cm^2 in molten NaOH at 320°C. The working electrode was initially passive in both cases (with Cl; E_{corr} =-272mV, without Cl; E_{corr} = -285 mV).

FUNDAMENTALS OF COATING SYSTEMS

STATUS REPORT

FOR

PROJECT 3674

March 22, 1990
Institute of Paper Science and Technology
Atlanta, Georgia

PROJECT SUMMARY FORM

DATE: February 26, 1990

PROJECT: 3674 - Fundamentals of Coating Systems

PROJECT LEADER: Cyrus K. Aidun

IPST GOAL:

Develop the technological foundation for the design of the next generation of high-speed coaters.

OBJECTIVE

To investigate the origin of nonuniformities in solid particle distribution, the instability of flow structure and the meniscus, and their effect on coat weight nonuniformities reported in high-speed high-solid concentration blade coating of paper and board.

FISCAL BUDGET: $80,000

RECENT PROGRESS

1) Results from the pilot coater trials have been analyzed and are presented below.
2) The formation of the high aspect ratio pigment particles on the paper have been studied for orientation preferences.
3) The required facilities for operation of laboratory equipment for coating experiments were not available for the most part of the last period. Much effort however, has been devoted to improving the equipment performance for quantitative measurements -- a deficiency of the previous experiments. Modifications and

improvements of the laboratory facilities will make accurate quantitative measurements possible for future studies.

CONTENTS

I. INTRODUCTION

Short dwell coaters (SDCs) enjoy several advantages over roll applicators. Contrary to roll coaters where frequent breaks occur at high speed (particularly with light weight papers), SDCs do not exhibit this problem and in principle can operate at ultra-high speeds. In practice, at high machine speeds SDCs experience runnability problems when the color viscosity exceeds a certain limit. Surface nonuniformities are the main obstacles which limit the maximum machine speed for high solids concentration in the coating color. We show here that the rheological properties coupled with the flow instability issues in various regions of the system play important roles in creating these limitations.

In high speed blade coating, surface nonuniformities can appear in the form of streaks and/or regions of high and low wet film thickness in MD and/or CD. Nonuniform structures, where the length scale is the same order of magnitude as the fluid/substrate

contact region, are categorized as macroscale. There are also problems with "randomly" spaced variations in surface coat weight which have small length scale characteristics and are independent of the base paper formation. Examples of miscoscale and macroscale nonuniformities are shown in Figures 1 and 2. Complete results from pilot coater trials are analyzed and presented in the next section along with a more complete scenario for the cause and origin of these nonuniformities. A possible explanation of the dynamics of the pilot coater trials with the short dwell coater is presented in ref. [1]. Section II reports the preliminary results of the study of particle orientation, interaction, and formation on the sheet.

During the last meeting, we showed that the time-periodic motion of fluid inside the puddle of a coating system can result in chaotic solid particle trajectories [2]. We have recently proved this claim by calculating the appropriate measures of the rate of divergence of neighboring particles (Lyapunov exponents). This work is continuing and more results will be available in future reports and articles.

In addition to flow instability and nonuniformities in coat weight distribution, most high-speed coating systems suffer from an additional constraint - air entrainment at the contact line between the coating liquid and the substrate. Some new results were presented in the last report [2]. This study is particularly relevant to the problems with fluid ejection from the pond of conventional size presses and will be continued within this context.

II. NONUNIFORMITIES WITH HIGH-SPEED SHORT DWELL-TIME APPLICATION OF COATING COLORS WITH CONCENTRATED SOLIDS

High aspect ratio clay particles (e.g., delaminated English China clay) in coating color provide a relatively superior surface quality for printing purposes. However, problems due to coat weight (CW) nonuniformities prevent application of these coating formulations at high solid levels (>58%) and desired machine speeds (~5000 fpm). It appears that because of the high aspect ratio disk-like geometry of the solid particles, the color viscosity easily exceeds 900 mPa.s which results in an upper limit on current application speeds. In general, with short dwell coaters (perhaps the most favorable

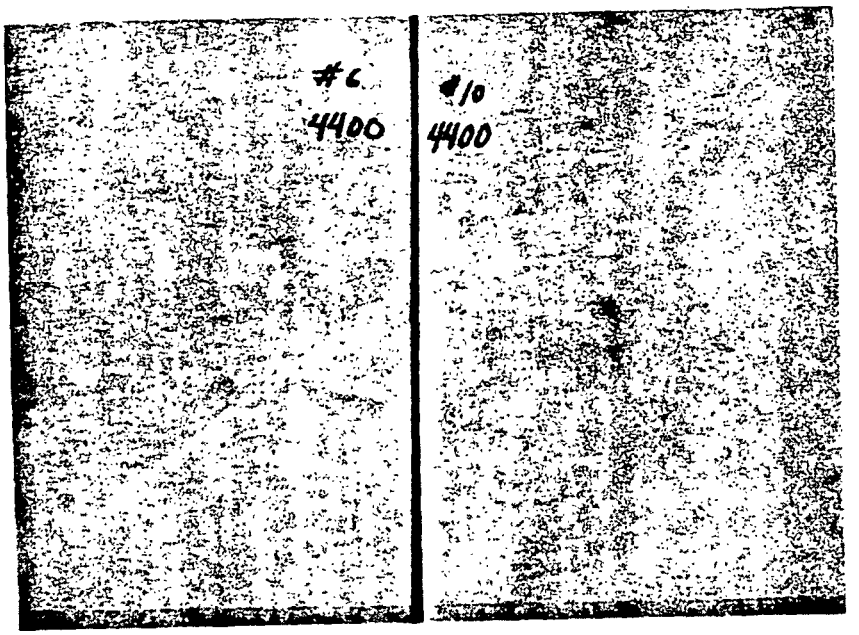

Figure 1. Macroscale nonuniformities in coat weight distribution for a LWC paper coated at 4400 fpm.

Figure 2. Microscale nonuniformities in coat weight distribution for a LWC paper coated at ~ 3500 fpm.

system for light weight coated products; i.e., <12 gsm) application of highly viscous colors will result in macroscopic nonuniformities in the cross-machine direction (CD). These nonuniformities appear in the form of visible streaks which run along the machine direction. These streaks signify regions (patches) of high and low coating weight concentration on the surface of the paper. Figure 1 is a good demonstration of these nonuniformities.

Through systematic pilot coater trials, we are documenting the influence of various parameters on the onset and severity of the CW nonuniformities. Laboratory experiments provide the fundamental physical information required to pinpoint the origin of this problem. The complete results from the pilot coater trials to date are presented in the next section. The results from laboratory experiments are included in the technical reports [1-4] and are not reported here.

II.2 Pilot Coater Trials

The results from the pilot coater trials are presented in this section. Here, the Reynolds number, Re, is defined as $VD\rho/\mu$ where V, D, ρ, and μ are the machine speed, length between the tip of the blade and the overflow baffle, color density, and the color viscosity, respectively. Pilot plant trials are based on actual production practices, the only difference being the effective span of the coater, which is only 40 cm (i.e., D/H =1, S/D = 10, where H and S are the hight and the span of the pond, respectively). In all trial runs reported here, operating conditions were adjusted to control coat weight, while the temperature of both the sheet and the color were maintained at about 27°C. Two series of trials were performed under well-controlled conditions using a 60-g/m^2 base stock for LWC in the first series of trials and a 50-g/m^2 stock in the second series. An outstanding difference between the two series was the type of delaminated clay used in otherwise similar formulations, i.e., typical of papers printed with rotogravure. English China and Georgia delaminated clays were used in the first and second series, respectively. In general, because coating colors are non-Newtonian fluids, it is difficult to determine with confidence the effective value of the Reynolds number in complex flow fields, such as the one inside the pond. Here, to be consistent with the flow visualization experiments, we have arbitrarily chosen to base the Reynolds number on the Brookfield (100 rpm) viscosity, μ.

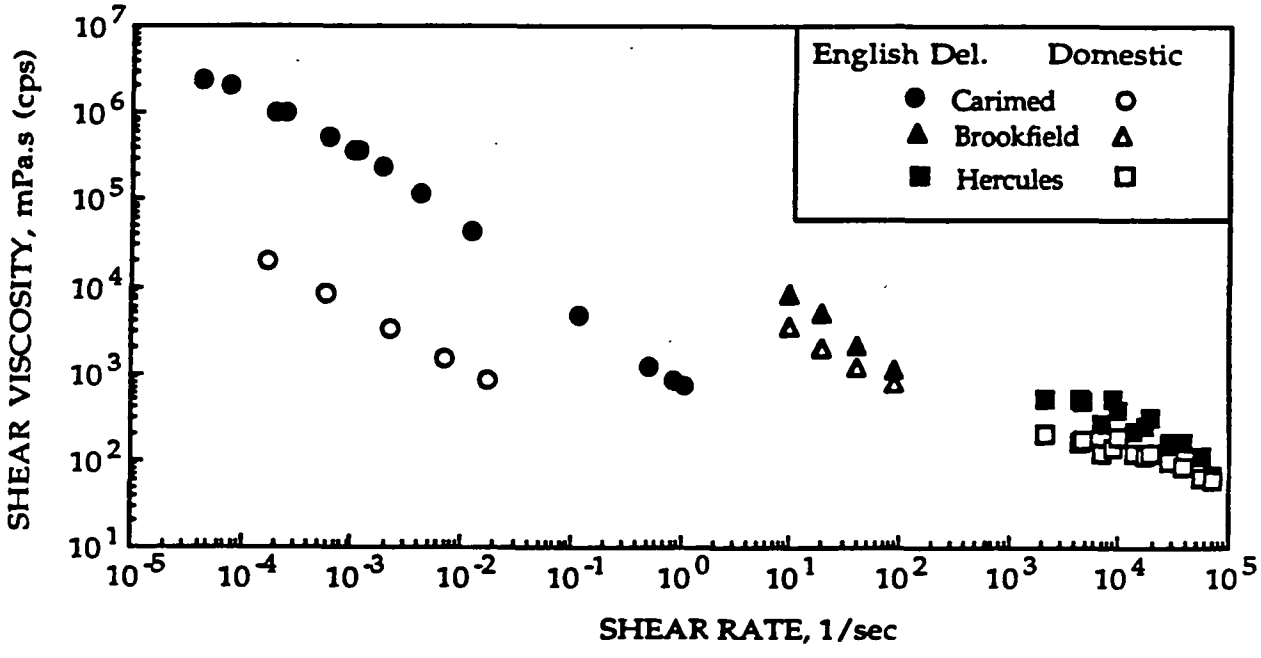

Figure 3. Rheological data of a typical color used in pilot plant trials and of the reference color. The first contains English delaminated clay, the second a domestic delaminated grade. Thermostatic temperature of Carimed and Brookfield data was 25°C, of Hercules data was 20°C.

The value of μ was controlled by maintaining high solids levels (56-59%) to keep it from falling below approximately 900-1000 mPa.s which, from previous experience, has resulted in visible streaks. It is worth noting certain rheological properties of the coating colors under consideration before presenting results from trials. In particular, we concentrate on formulations containing pigments with relatively high aspect ratio particles (i. e., above 15 to 1), such as English delaminated grades which are composed of particles plattier than those in domestic delaminated grades of clay. In addition to 100 percent delaminated clay, the rotogravure formulation contained 3.0-4.5 pph SBR latex and 0.3 pph alkali-swellable thickener, and its total solids content was approximately 58% by weight based on dry pigment.

Figure 3 demonstrates the relationship between viscosity and shear rate for ten decades of shear using three different viscometers [3]. The data points with the formulation described above are compared to a reference color, containing a domestic grade of delaminated clay at 61% solids that had no visible runnability problems for machine speeds up to 1200 m/min (4000 fpm).

Two different coating colors were applied on light weight stocks using a typical short dwell head. Composition of each coating color is given below (pph=parts per hundred of pigment by weight).

Trial A

Stock:	60 g/m^2
Color formulation:	
Delaminated English China clay - type A	77%
Delaminated English China clay - type B	33%
Dispersant (tetrasodium pyrophosphate)	0.35 pph
Lubricant (sodium stearate)	0.50 pph
Latex (styrenebutadiene emulsion)	4.5 pph
Thickening agent (alkali-swellable emulsion)	0.26 pph
800 ml Ultraviolet dye	
200 ml NaOH to control pH to 9.0	

Trial B

Stock:	50 g/m^2
Color formulation:	
Delaminated Georgia kaolin clay	100%
Dispersant (tetrasodium pyrophosphate)	0.35 pph
Lubricant (sodium stearate)	0.50 pph
Latex (styrenebutadiene emulsion)	4.5 pph
Thickening agent (alkali-swellable emulsion)	0.26 pph
800 ml Ultaviolet dye	
200 ml NaOH to control pH to 9.0	

The following conditions were used in both trials:

Blade bevel = 45 degrees
Blade length = 76 mm
Blade thickness = 0.5 mm
Blade stickout = 1.9 cm
Head angle = 54 degrees
Baffle Gap = 3 mm

The results from the trials are presented in tables 1 and 2 below:

TABLE+ 1. Trial A

Sample Code	0	1	2	3	4	5	6	7	8
Coat Weight (gsm)	11	11	11	11	11	11	11	11	11
Total Solids (% by weight)	58.1	58.1	56.6	56.6	56.6	56.6	57.6	55.6	55.6
Reel Moisture (%)	4.5	4.5	4.5	4.5	4.5	4.5	4.5	4.5	4.5
Tube Pressure (kPa)	207	90	131	138	152	138	97	90	97
Feed Pump Rate (L/min/m)	166	166	166	166	166	166	166	166	166
Chamber Pressure (kPa)	–	10	10	10	10	10	9.5	9.5	9.5
Machine Speed (m/min)	1070	305	762	793	823	732	610	640	671
Color Viscosity (mPa s)									
Low-shear	1884	1884	1428	1428	1428	1428	1412	980	980
High-shear	73	73	66	66	66	66	63	49	49
Color Temperature (°C)	26.7	26.7	28.9	28.9	28.9	28.9	33.3	27.8	27.8
Reynolds Number, Re	729	207	687	714	742	659	556	841	881
Comments	Severe Streaks	No Streaks	Streaky	Streaky	Streaky	Streaky	No Streaks	Streaky	Streaky

Trial A cont'd

Sample Code	9	10	11	12	13	14	15
Coat Weight (gsm)	11	11	11	11	11	11	11
Total Solids (% by weight)	55.6	57.1	57.1	57.1	57.1	56.3	56.3
Reel Moisture (%)	4.5	4.5	4.5	4.5	4.5	4.5	4.5
Tube Pressure (kPa)	104	110	117	97	104	104	173
Feed Pump Rate (L/min/m)	166	166	166	166	166	166	166
Chamber Pressure (kPa)	9.5	9.5	9.5	10	10	10	10
Machine Speed (m/min)	701	610	701	488	549	610	1067
Color Viscosity (mPa s)							
Low-shear	980	1236	1236	1236	1236	1056	1056
High-shear	49	58	58	58	58	56	56
Color Temperature (°C)	26.7	28.9	28.9	28.9	28.9	27.8	27.8
Reynolds Number, Re	921	635	730	507	571	743	1300
Comments	Streaks	Streaks	Severe Streaks	No Streaks	Sporadic Streaks	Streaks	Severe Streaks

+ Streaks do not appear (at least visually) under these conditions when formulations with lower viscosity are used.

TABLE+ 2. Trial B

Sample Code	1	2	3	4	5	6	7	8	9
Coat Weight (gsm)	6.2	6.4	6.4	6.2	6.2	6.8	6.5	6.3	7.0
Total Solids (% by weight)	59.6	59.6	59.6	59.6	59.6	59.6	59.6	59.6	59.6
Reel Moisture (%)	–	3.6	4.4	4.7	5.3	5.9	2.5	3.3	5.9
Tube Pressure (kPa)	221	200	200	200	200	214	152	159	207
Feed Pump Rate (L/min/m)	166	200	166	166	166	166	200	166	166
Chamber Pressure (kPa)	9.5	10	10	10	10	10	8.0	9.0	9.0
Machine Speed (m/min)	701	305	762	793	823	732	305	640	671
Color Viscosity (mPa s)									
Low-shear	1268	1292	1268	1280	1292	1224	904	1012	1052
High-shear	62.5	–	–	–	–	–	–	–	–
Color Temperature (°C)	25.6	25.6	25.6	25.6	25.6	25.6	25.6	25.6	25.6
Reynolds Number, Re	790	670	850	910	1000	1240	480	860	1650
Comments	Severe Streaks	No Streaks	Streaky	Streaky	Streaky	Streaky	No Streaks	Streaky	Streaky

Trial B cont'd

Sample Code	10	11	12	13	14	15
Coat Weight (gsm)	6.3	6.5	6.0	6.2	6.7	6.3
Total Solids (% by weight)	59.6	59.6	59.6	59.6	59.6	59.6
Reel Moisture (%)	5.4	2.6	2.7	3.1	3.9	4.4
Tube Pressure (kPa)	221	159	159	145	145	145
Feed Pump Rate (L/min/m)	200	200	200	200	200	200
Chamber Pressure (kPa)	10	10	10	10	10	10
Machine Speed (m/min)	1340	366	428	488	549	610
Color Viscosity (mPa s)						
Low-shear	1004	1104	1120	1156	1160	1156
Color Temperature (°C)	24.4	24.4	24.4	24.4	24.4	24.4
Reynolds Number, Re	1900	471	542	600	673	750
Comments	Severe Streaks	No Streaks	Streaky	Streaky	Streaky	Streaky

+ Streaks do not appear (at least visually) under these conditions when formulations with lower viscosity are used.

The above results suggest a connection between the appearance of streaks on the coated web and the Reynolds number, Re, for the range over which fluid viscosity and machine speed are varied. Generally, the Reynolds number decreases with reduced machine speed, but increases with lower fluid viscosity. Good examples of this are trials 6, 10, and 14 in the first series where constant machine speed at 610 m/min (2000 fpm) may or may not produce streaks depending on viscosity and the value of Re. By comparing these with, for example, sample 15 of Trial B, we conclude that this effect is not dependent on the specific type of clay pigment used. Also comparison of runs 2 to 6 show that increasing the machine speed while maintaining constant viscosity induces streaking. These results show that independent of how a certain value of Re is attained, streaks will appear if its value exceeds a critical number. Runs 2 and 14 in trial B give a value of Re ~ 670 for the onset of streaks.

The range of Re over which streaks definitely occur for the first time, i.e., 550-750, is in the same order of magnitude where the initial laminar transitions from steady state to time-periodic and more complex states have occured in flow visualization experiments with the driven cavity [2,3]. Direct and quantitative comparisons between the two studies are only possible when the effects of geometry (i.e., spanwise aspect ratio) and fluid rheology are considered in future studies.

The above results show that among all of the parameters, the Reynolds number appears to be the single controlling factor for the occurrence of streaks. It should be noted, however, that the behavior of the system changes dramatically when the color viscosity falls below about 900 (mPa.s). In other words, in any of the above trials where streaks appear, if the viscosity is reduced below this number the streaks disappear even though the Reynolds number increases. This shows that at high viscosities or high solids concentration, the flow patterns resulting from hydrodynamic instability in the pond, presented in the last report [1], are coupled to other factors. These could be the rheological properties of the coating color, geometric factors, and/or particle orientation properties. We are considering several scenarios that would explain the results and the observations from the pilot trials. One based on flow pattern formation and particle orientation is given below.

Because of the recirculating flows in the pond, fluid elements and other components of coating colors that are only few millimeters away from the web move opposite to the machine direction. Only after these particles have penetrated the viscous layer that forms on the moving web when the color contacts it upstream, do they experience the viscous drag of the substrate, at which point they are accelerated and convected downstream. In systems with an applicator roll, the outer layer of the flow which deflects down the blade is irrotational (see the next section). In contrast, the flow in short dwell coaters (or in fact any surface application system with a pond [1]) contains recirculating eddies which become unstable due to centrifugal forces. This gives rise to time-periodic and three-dimensional flow patterns. Cellular structures in the pond cause nonuniform orientation of pigment particles and, if there is not enough time for the particles to reorient, the structures can create unstable conditions in the nip. As pointed out by Gane and Coggon [4], orientation phenomena of clay particles upstream of the blade can also affect the final coating properties. Such effects are generally more pronounced in formulations containing highly asymmetric particles, e.g., delaminated clays, at relatively high solids content. They may not, however, be important when using pigments with small particle size, e.g., a no. 2 grade of clay. Thus, CD profile variations can be attributed to the hydrodynamics in the pond coupled with color properties, which are proportional to viscosity. This scenario explains why the streaks disappear below a certain solid concentration, and, it explains the appearance of streaks with larger aspect ratio solids. Other equally reasonable scenarios are also being studied.

II.3 Blade Coaters with Roll Applicator and Short Dwell Pond: A Comparison

Consider the flow in a blade coating system with a roll applicator (Fig. 4a). Various sections of the flow field exhibit unique characteristics. Here, the web is moving from left to right carrying a thick layer of fluid with it. The fluid in this layer (region 1) moves like a solid body and experiences almost zero shear. As this layer approaches the blade it bifurcates into roughly three streams. Stream A, adjacent to the web, continues into the nip of the blade (region 6) and experiences an enormous increase in shear rate. Layer B, the middle stream, falls just below the separation line (region 11), turns downward and forms two boundary layers, one on the flat surface of the blade (region 12) and a second next to the concave

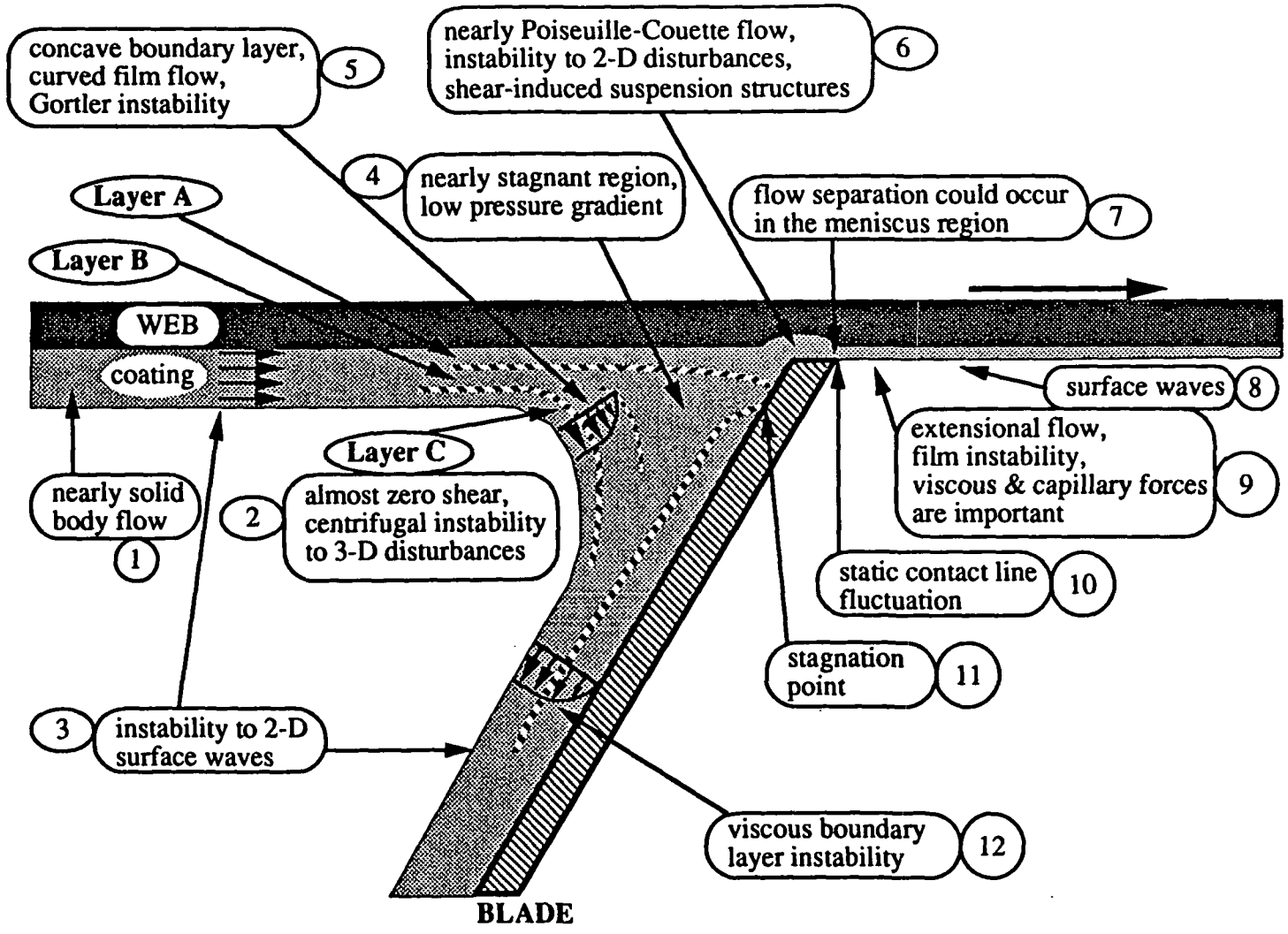

Fig. 4a Some stability characteristics of flow in blade coating with a roll applicator.

region of layer C. The free-surface stream (layer C) reflects down the blade under negligible viscous forces (irrotational flow).

In an incompressible fluid (e.g., coating color), a disturbance at one section propagates instantaneously throughout the media. Therefore, if three-dimensional disturbances grow upstream of the blade, their effects will propagate through the blade tip and may result in coat weight nonuniformities (streaks, ...). Let us then casually investigate the stability properties of the three layers mentioned above.

Layer A enters a high-shear region under the blade and follows a nearly Poiseuille-Couette velocity distribution [6]. The first instability will be due to a two-dimensional disturbance mode in the plane of the base motion, the Z-MD plane. Further downstream in the meniscus region of the blade tip, however, other mechanisms such as visco-capillary instabilities become important.

The irrotational stream (layer C) is under a centrifugal force and could become unstable to three-dimensional disturbances. According to Rayleigh's criterion [1], if the radial gradient of the magnitude of the angular momentum becomes negative, then the flow could become unstable. The most critical region of this layer is the curved section which is nearly circular. Let $r = R_1$ and $r = R_2$ define the radius of the inner and outer boundaries of this region, respectively. The azimuthal component of velocity, u_θ depends most strongly on r alone. The criterion for stability reduces to

$$\frac{r}{u_\theta}\frac{du_\theta}{dr} > -1.$$

This presents an approximation for the stability criterion of layer C. A more accurate stability analysis can be obtained by actually calculating the conditions for instability along the streamlines given by numerical simulations [6].

Between layers B and C in the curved section of the stream (region 12), the velocity rapidly decreases to zero forming a concave boundary layer susceptible to Görtler-Taylor type instabilities [1]. This boundary layer, in conjunction with layer C, roughly forms a free-

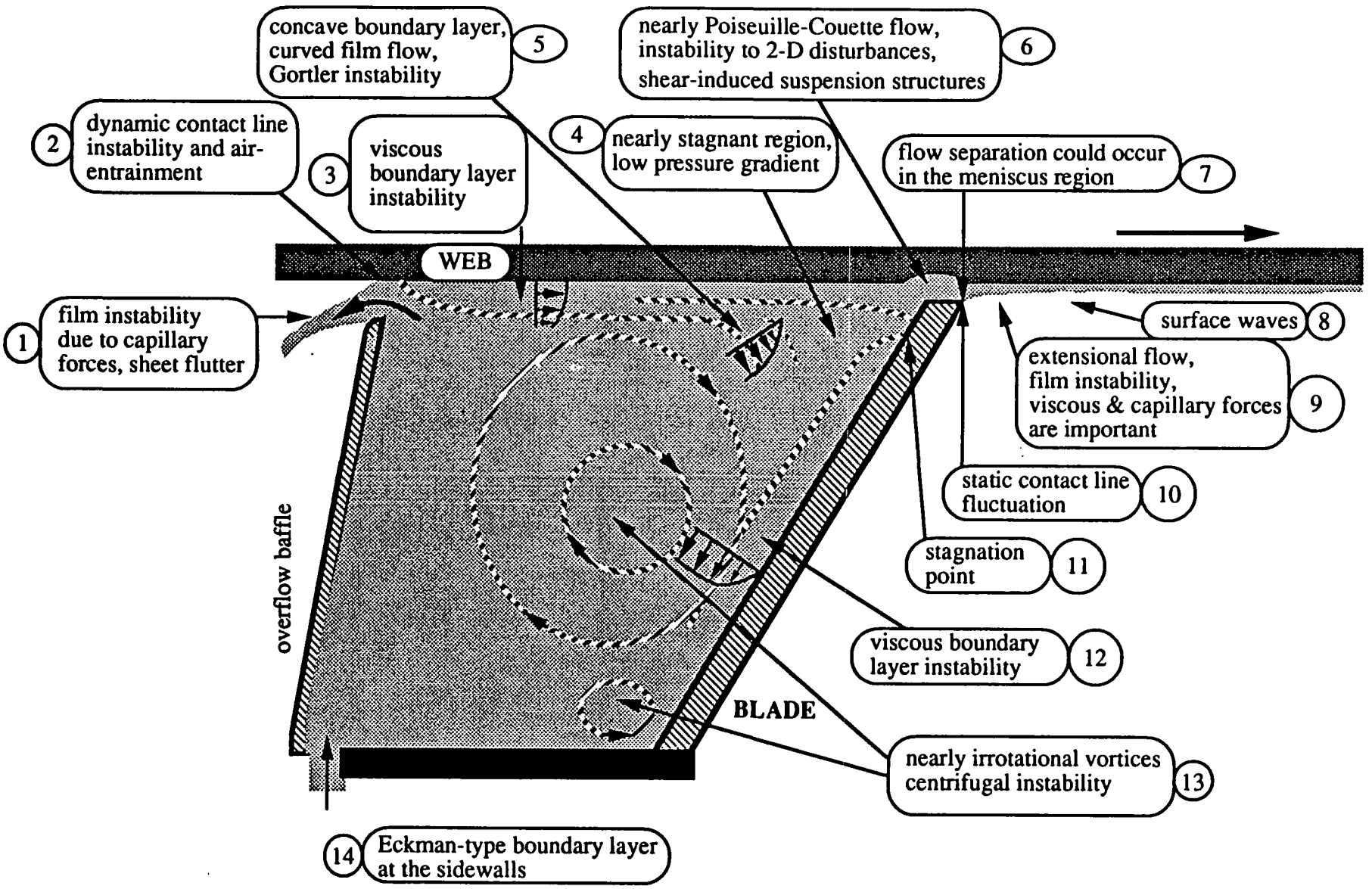

Fig. 4b Some stability characteristics of flow in blade coating with a short dwell time applicator.

surface curved film. This flow is similar to a free-surface film flow down a concave wall which could become unstable to Görtler-type vortices in the concave region [7]. The critical Reynolds number, $Re \equiv \frac{U_0 \delta}{\nu}\left(\frac{\delta}{R}\right)^{1/2}$, (based on the radius of curvature, R, film thickness, d, and the average film velocity, U_0) for onset of Görtler-type vortices for the case of a film falling under gravity is reported [7] to be about 16.1 which is close to the value of 15.8 for the onset of Görtler instability in a boundary-layer over a concave wall.

A blade coating system with puddle or short-dwell applicators (Fig. 4b) has somewhat different stability properties compared to the system considered above. In addition to the local instability discussed above, the *apparent two-dimensional* flow in the pond of these systems can be globally unstable. In fact, the flow of Newtonian fluids in a cavity simulating the pond of a short-dwell coater is shown to have multiple stable steady states [2,4]. This proves that it is quite possible that a short dwell coating system can operate at different flow states with the same machine speed. This important physical property, if explored in more detail, can in fact be controlled and used with significant advantages. Although a direct correlation between the results from laboratory flow visualization experiments (with a cavity of span ratio S/D=3) and the pilot coater trials (S/D=10) is not possible because of geometric differences, the qualitative results presented here show that, in general, the pond hydrodynamics significantly influence the coat weight profile. The potential of controlling the dynamics of the coating system at a given machine speed warrants an indepth and quantitative investigation of the influence of geometry on the hydrodynamic stability properties of flow in the pond upstream of the blade.

III. MICROSCALE ANALYSIS OF PARTICLE ORIENTATION/INTERACTION

In blade coating, the coating color under the blade experiences an enormous amount of shear (10^5-10^6 sec^{-1}). Experiments indicate that when a high concentration of solid particles in a coating color is placed under large shear in a narrow gap, the particles tend to cluster into patches forming a bridge between the two boundaries of the gap. Figure 5 illustrates this behavior. Transformation of these clusters onto the surface of the coated paper results in nonuniformities and deterioration of the surface quality.

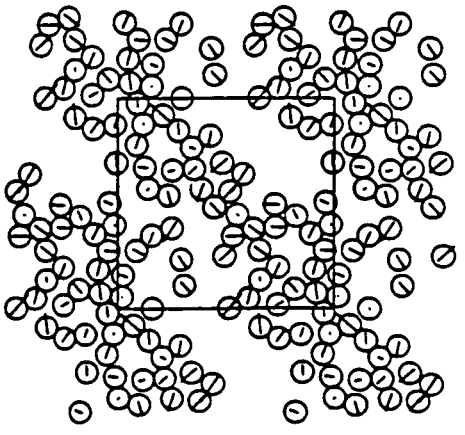

Figure 5. Shear-induced string-like structure in solid suspensions.

Dynamic Light Scattering techniques can be used to study the distribution of solid particles under shear. Light scattering studies of solid particles in a liquid subjected to steady and oscillatory shear flows have shown evidence of "string" structure with length scales comparable to the microstriations reported in high speed coating of paper.

To study the effects of particle-blade interactions and particle orientation effects, we can take two approaches: 1)systematic experimental observation of the clay particle formation on the surface of the coated sheet, and 2) analysis of fundamental governing physical principles. The first approach, which includes Scanning Electron Microscope (SEM) analysis of the paticle formation on the surface and examination for orientation preferences, is underway and preliminary results are reported below.

The second approach involves computational analysis of the particle dynamics coupled with momentum conservation equations. For coating colors where particles are suspended in a fluid medium, the Navier-Stokes equation applies to the fluid phase, while the Langevin system of equations describes the motion of the particles. For a problem with N-particles, the Langevin system consists of N-coupled equations which govern the translation and rotation of each particle under a) hydrodynamic forces exerted on the particle due to their relative motion to the fluid, b) the deterministic non-hydrodynamic forces which could be either interparticle or external, and c) the stochastic forces that give rise to Brownian motion. We may consider this approach in future studies.

III.1 Experimental Investigation of the Particle Orientation on a Coated Surface

The high aspect ratio solid particles always have a tendency to orient in such a way to minimize drag. This is the reason that three-dimensional flow patterns inside the pond align the high aspect ratio clay particles in a differential orientation in CD. It is not clear if the oriented particles formed inside the pond remain oriented after passing through the blade nip. If so, then the orientation effects of the particles and their interaction with the blade contribute to the nonuniformities and formation of streaks on the surface of the paper.

Samples from the pilot coater trials are being analyzed to understand the orientation and formation of the particles and to obtain information in the microscale levels. Figures 6 and 7 are SEM pictures of coated surfaces from sample 0 of trial A at x2000 and x120 magnification, respectivley. These pictures focus on the edge of a streak, since the possibilty of observing variations is greatest in that region.

The clay particles are clearly visible in Figure 6. The preliminary studies with the image analyzer have not shown conclusive orientation effects. Figure 9, however, reveals an interesting effect. It appears that fine streak lines have formed at about 20 degrees from the machine line. Is this caused by the fiber orientation of the substrate ? Figure 8 is a x120 exposure of the uncoated substrate used in Trial A. Since the fibers do not have the same orientation, the microscale streaks are most likely due to the coating system and not fiber orientation. Then why would the fine scale streaks form an angle with MD?

The location analyzed in Figures 6 and 7 is at the edge of a patch of streak which is about 2 feet in length. This location is also about half an inch from the leading point where, as demonstrated in Figure 9, the macroscale streak forms an angle roughly 20 degrees from the machine line. Then the fact that particle formation at a microscopic level correlates with the macroscopic formations suggests the possibility that the alignment of particles in the pond is due to three-dimensional flow patterns and their translation through the blade nip and onto the surface of the sheet. More SEM analyses are underway to examine these phenomena.

FUTURE PLANS

Future experiments will focus on quantitative measurements of flow rate and the fluid velocity field, information required to determine the stable operating conditions for SDCs.

The cavity used in laboratory experiments has a span aspect ratio of 3 to 1 (i.e., S/D = 3) which is much smaller than a typical SDC coater (S/D > 10). The effects of geometry on the dynamics of flow in the pond will be studied by using cavities with larger span aspect ratios.

Studies of the effects of suspension rheology, shear-thinning, and particle interactions and formation on the stability properties and coat weight nonuniformities will be further explored using

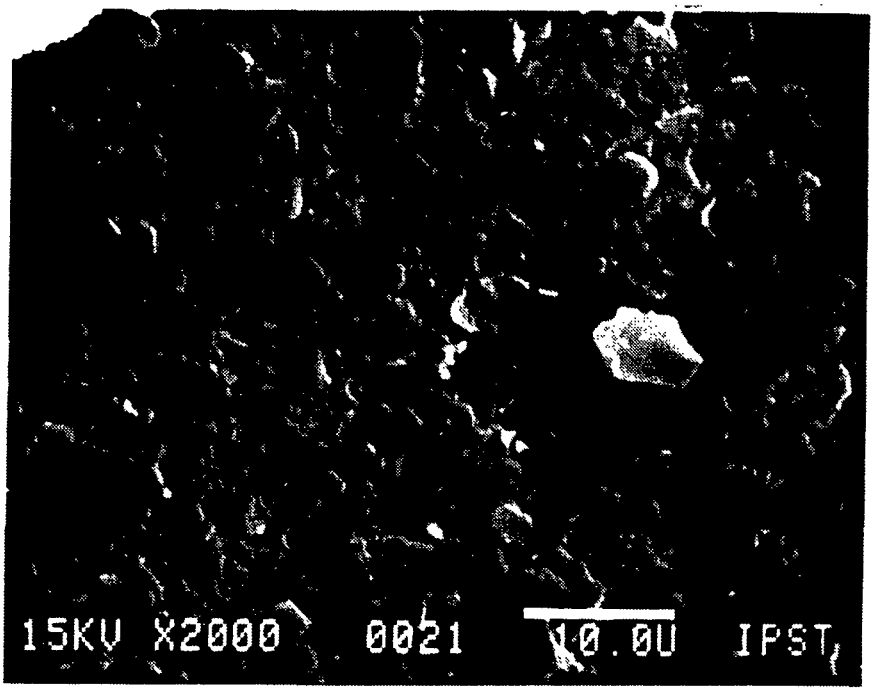

Figure 6. SEM picture of the coated surface at 2000 magnification (for location see Figure 9).

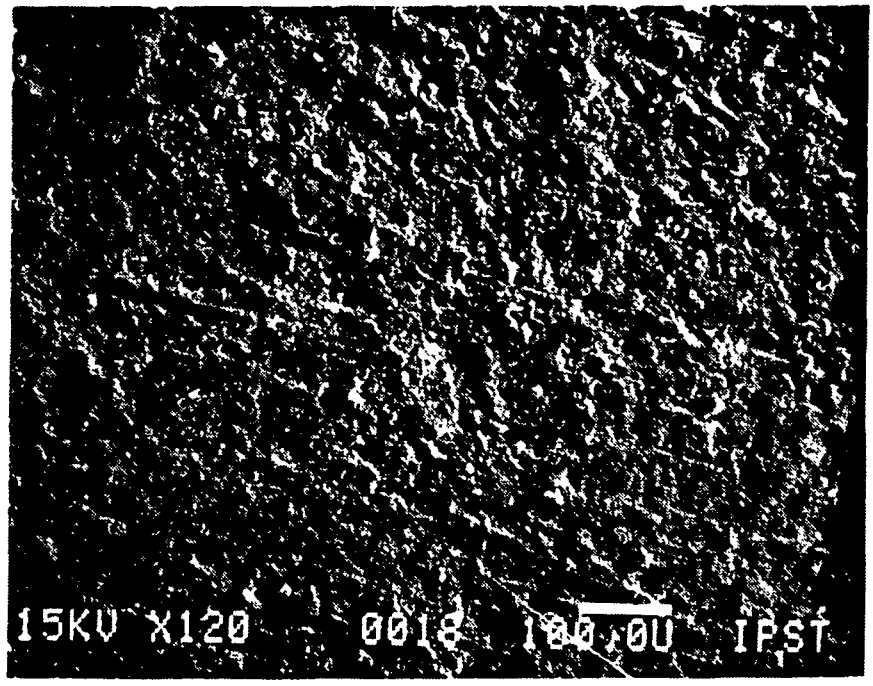

Figure 7. SEM picture of the coated surface at 120 magnification (for location see Figure 9).

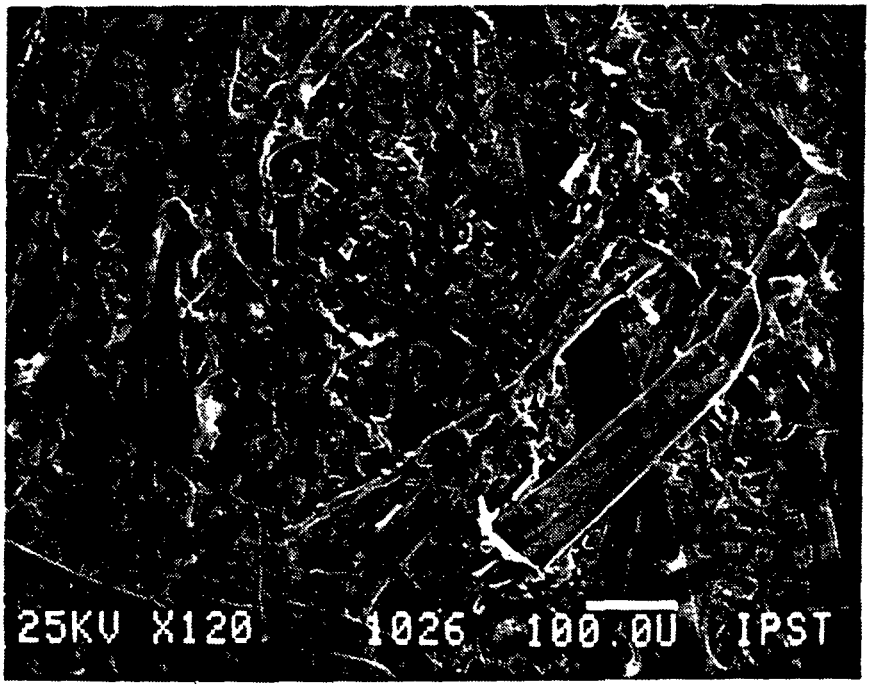

Figure 8. SEM picture of 120 magnification of the uncoated paper used in Trial A of the pilot scale experiments.

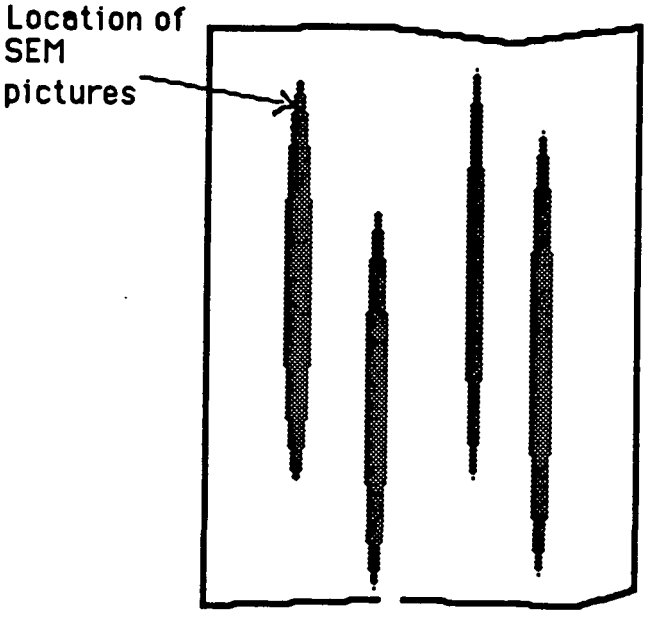

Figure 9. Schematic of the location of SEM pictures in Figures 6 and 7.

SEM and image analysis techniques. With increased manpower, more time will be spent on computational analysis -- a particularly promising tool for this study.

Air entrainment studies are in progress. The apparatus for this study consists of a roll immersed halfway in a pool of liquid. Rotation of the roll generates a dynamic contact line which destabilizes and results in air entrainment at some critical roll speed. The effect of fluid viscosity, surface tension, and roll surface properties on the air-entrainment mechanism is under investigation. Initial results reported briefly during the last meeting [2] have been particularly useful for understanding the fluid ejection problems in size presses. This work will continue and will be extended to further investigate the air-entrainment and its interaction with the flow in the pond of size presses.

SIGNIFICANCE TO THE INDUSTRY

High quality coated paper products are a significant segment of the total paper market. The goal of this research project is to contribute to the development of a cost- effective coating process for products with superior quality and more flexibility. This will provide the industry with a competitive edge in an ever growing market.

REFERENCES:

1. Aidun, C.K., "Principles of Hydrodynamic Instability in Coating Systems," Technical Report, Institute of Paper Science and Technology, 1990; also will be presented at the 1990 TAPPI Coating Conference.

2. Aidun, C.K., Institute of Paper Science and Technology, Project 3674- Fundamentals of Coating Systems, Status Report to PAC, pages 51-71, October 1989.

3. Triantafillopoulos, N.G., and Aidun, C.K., "Relationship between flow instability in short dwell ponds and cross directional coat weight nonuniformities," Technical Report, Institute of Paper Science and Technology, 1990; also will be presented at the 1990 TAPPI Coating Conference.

4. Aidun, C.K., and Triantafillopoulos, N.G., "Global stability properties of flow structures in the pond of a short-dwell blade coater," Int'l Symp. Mech. of Thin-Film Coating, AIChE Meeting, March 18-22, 1990.

5. Gane, P.A.C., and Coggon, L., "Coating Blade Geometry: Its Effect on Coating Color Dynamics and Coated Sheet Properties," *Tappi*, 87-96, 1987.

6. Pranckh, F.R., and Scriven, L.E., "The Physics of Blade Coating of Deformable Substrate," 1988 Coating Conference Proc., TAPPI Press, Atlanta, GA, 1988.

7. Schweizer, P.M., and Scriven, L.E., "Evidence of Görtler-Type Vortices in Curved Film Flows," *Phys. Fluid*, **26**, 619, 1983.

X-RAY STUDIES OF WEB CONSOLIDATION

STATUS REPORT

FOR

PROJECT 3684

March 22, 1990

Institute of Paper Science and Technology
Atlanta, Georgia

PROJECT SUMMARY FORM

DATE: February 26, 1990

PROJECT: 3684 - X-Ray Studies of Web Consolidation

PROJECT LEADER: Cyrus K. Aidun

IPST GOAL:

Develop a novel technique for direct visualization and measurement of web consolidation. Enhance the performance of web consolidation in terms of property development and dewatering.

OBJECTIVES

Develop a fundamental understanding of sheet deformation in wet pressing through direct experimental visualization and measurement of the dynamics in the nip of a roll press. Apply the fundamentals to improve the commercial web consolidation processes.

FISCAL BUDGET: $120,000

SUMMARY OF RECENT PROGRESS

Progress in this project has been nearly halted due to the unavailability of a lead-lined room for x-ray studies. Construction of this room is expected to start shortly. In anticipation of this delay, several x-ray pictures were accumulated before relocation and have been studied with the image analyzer. Although this preliminary study proves the feasibility of this technique for sheet deformation and multilayer sheet formation studies, further advances in the technique are required before we can analyze light weight sheets with sufficient accuracy. The present technique, however, can be applied to paperboard and multilayer sheet formation studies.

CONTENTS

I. INTRODUCTION

Web consolidation theories currently available are mainly based on indirect measurements and speculation. In this project, we use the flash x-ray imaging in conjunction with image analysis techniques to generate direct results on the fluid flow and property development in wet pressing and impulse drying. An image analyzer at the Institute will be used to obtain quantitative results on local sheet deformation, densification, and dewatering.

Wet pressing, impulse drying, or any other process which involves fluid flow in a deformable porous media share a common feature -- coupling between the fluid flow and the deformation of the medium. The technique we are using in this study allows direct measurement and analysis of this behavior. Detailed analysis of the relation between the sheet deformation (strain gradient in normal as well as lateral directions) and the fluid flow is the key to understanding and controlling the property development and dewatering behavior in web consolidation.

II. BACKGROUND

When an inhomogeneous medium is exposed to x-ray radiation, components with different x-ray absorption coefficients will produce a contrast image. For example, a sheet of paper will absorb less radiation than a metallic sheet.

By placing small solid x-ray tracers (particles, fibers, or continuous wires) in a sheet of paper, we are able to capture their displacement before and after pressing by superimposing two x-ray images -- one image of the sheet before compression, and one after. An exaggerated example is shown in Figure 3, where spherical metallic particles are sandwiched between several sheets. Because of reproduction of the image, the particles cannot be seen in Figure 3b; however, they can be seen in the original x-ray radiograph. A more realistic image is shown in Figure 4. Using the image analyzer, we then label each particle and measure its relative displacement in all directions. This information gives a direct measure of the local strain gradient tensor (i.e., local deformation in all directions). The local strain tensor and local hydraulic pressure can then be calculated. These results would be useful in understanding the dewatering mechanisms in wet pressing and web consolidation processes in general.

III. PROGRESS TO DATE

An experimental roll press has been designed and constructed for the flash x-ray studies. It consists of 6" diameter, 1" thick rolls with maximum operating speed of 300 ft/min. The value of the nip pressure is dependent on the thickness of the sheet and the felt. The relative positions of the x-ray unit with the rolls and the x-ray film cartridge are shown in Figures 1 and 2. The x-ray radiation source is a Hewlett-Packard Model 43733A Flash x-ray unit.

Currently, the impulse drying simulations use a commercial propane soldering torch to heat the upper roll to a maximum temperature of 550°F. Either liquid silver nitrate could be applied directly on the surface of the sheet before it enters the nip or x-ray tracers (solid, liquid, or both) could be added to the sheet during forming.

For quantitative studies, we adopt the second approach -- that is x-ray tracers in the form of solid particles, encapsulated fluids, or fibers are carefully placed in a sheet. By recording their x-ray images before, during and after the pressing process (be it wet pressing or impulse drying), we are able to obtain direct quantitative results on local and directional sheet deformation and fluid flow.

Small spherical solid particles (20 to 100 microns in diameter), continuous thin wires (~ 25 microns), and metallic fibers (~ 25 microns in diameter, 1 mm long) have been used. An image analyzer is used to enhance the contrast in the x-ray image and assist in measuring the local deformation of the sheet. This process is demonstrated in Figures 4 and 5. The first figure is an x-ray image of Tungsten particles in a sheet, and the second figure is the same picture when magnified and processed by the image analyzer.

The actual particles are smaller than their enhanced (in contrast) image in Figure 5. This is partly because of the relatively poor resolution of the x-ray film which causes a blurring effect. In actual measurements, the image analyzer will be used to pinpoint the center of mass of each particle and to measure their relative distance from each other and from the rolls.

Figure 6 shows the enhanced x-ray image of three 25 micron tungsten wires implanted in a sheet of paper (~ 30% solids). Here the wires are also much smaller than their enhanced image.

By optimizing the roll press with the x-ray system, fine tuning the x-ray film development procedure, and using the image analyzer to enhance contrast, we expect to greatly improve the quality of future x-ray images. In fact, the optimization studies currently underway have already shown improvements in contrast and resolution.

These can be seen from the static and dynamic x-ray images of multilayer sheet formation studies. Although we are currently in the preliminary stages of this work, the initial images have shown sufficient resolution for accurate measurements in sheet deformation. An example is shown in Figures 7 and 8 where three rows of 50 micron tungsten fibers are sandwiched between four layers of sheet which are placed over a standard Nomax felt. The sample in Figure 7 is under zero pressure and is used as a

reference. Figure 8 is a picture of the same sample as it is being pressed approximately 680 psi at a roll speed of about 100 fpm. By comparing these images and measuring the displacement of the fibers, we measure the deformation of each layer and the shear or slip between layers.

FUTURE PLANS

Investigate the impact of the mechanics of sheet densification in multi-layer sheet forming by examining the local densification and relative shear via x-ray imaging technique.

The technique needs to be further developed in the following steps:

1. Enhance the roll press instrumentation for more accurate measurements and control of pressure and roll speed.

2. Explore the possibility of increasing the x-ray resolution and contrast by modification of the FXR tube.

SIGNIFICANCE TO THE INDUSTRY

Even modest improvements in the dewatering processes are extremely important to capacity, drying energy reduction, better property development, and removing bottlenecks. Understanding the interaction between the fluid flow and the deformation of the porous network could lead to improved property control, enhanced dewatering, reduced drying energy and increased capacity.

a)

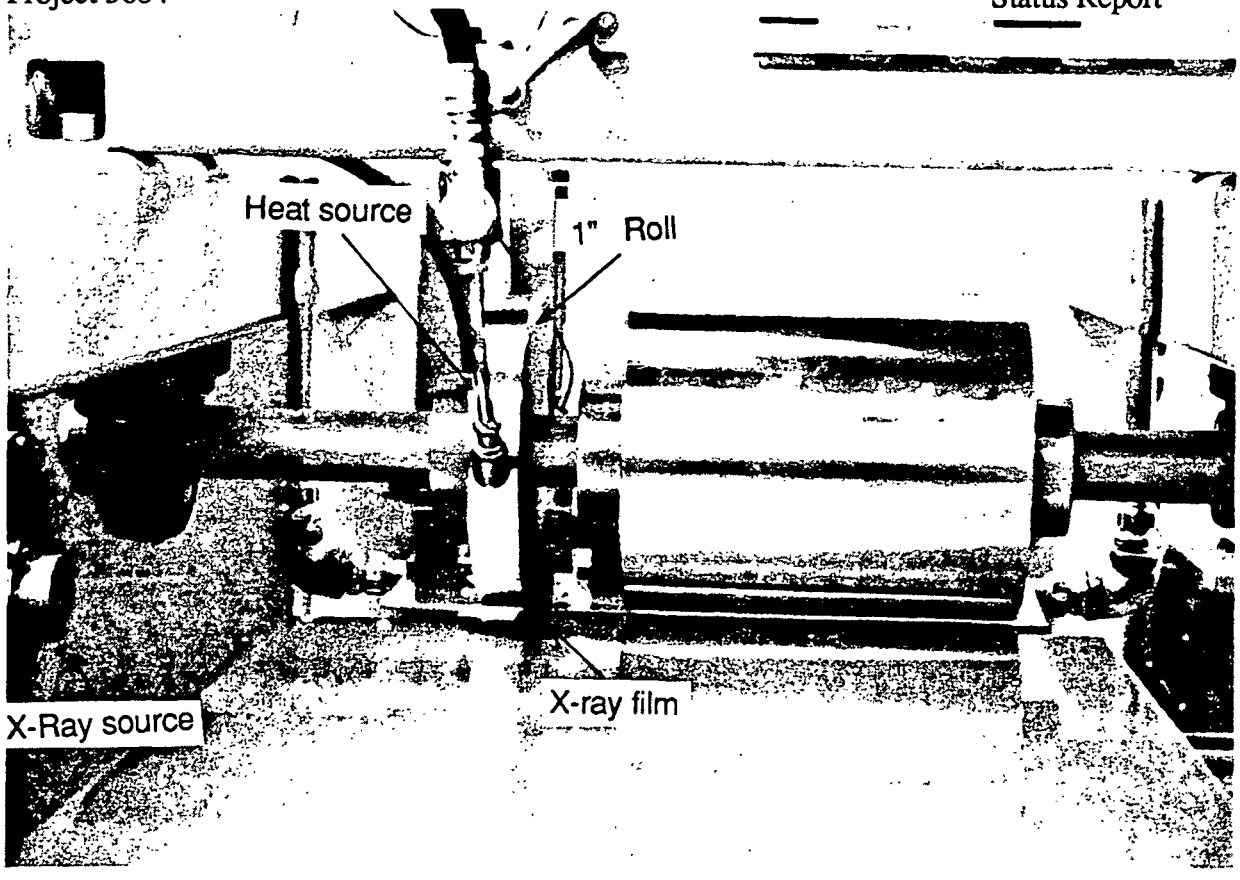

b)

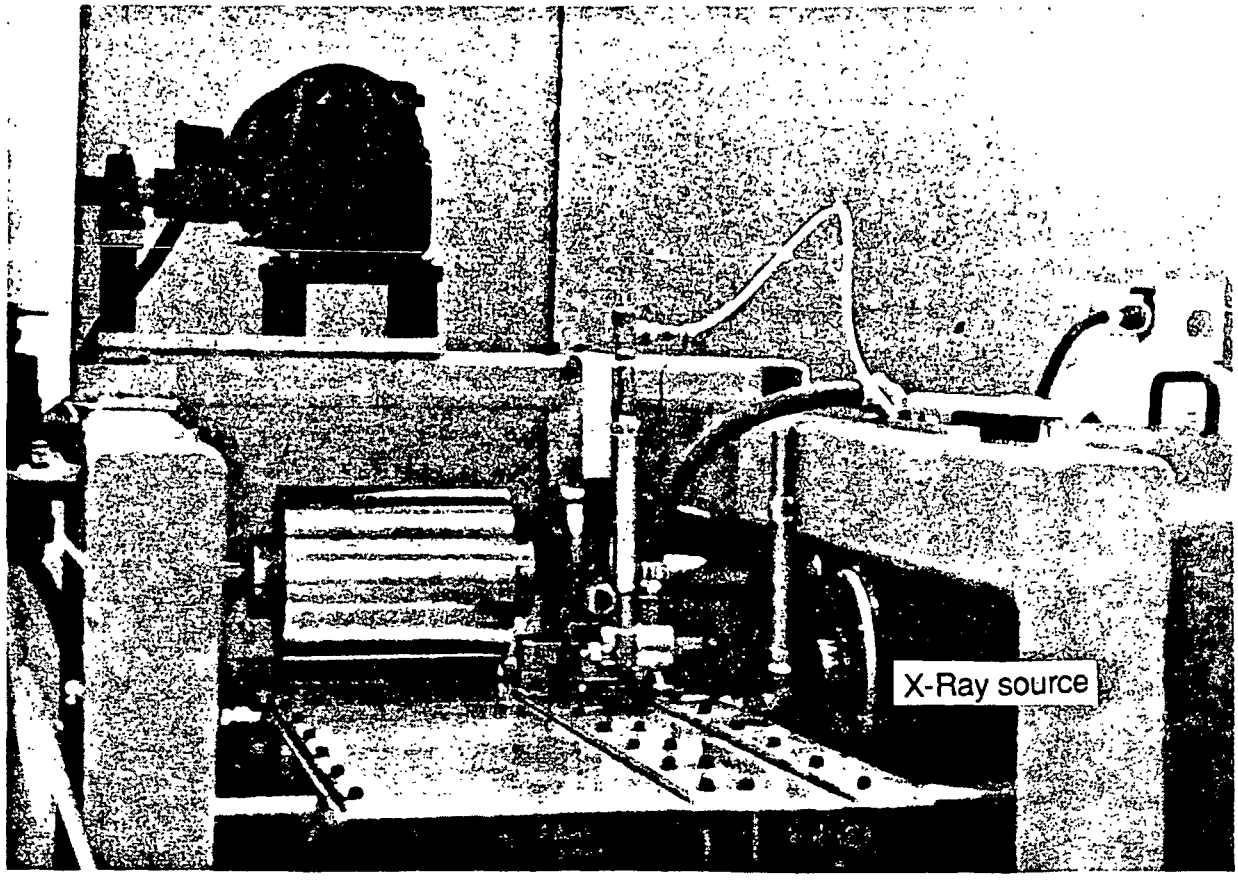

Figure 1. X-Ray Roll Press a) exit side b) entering side

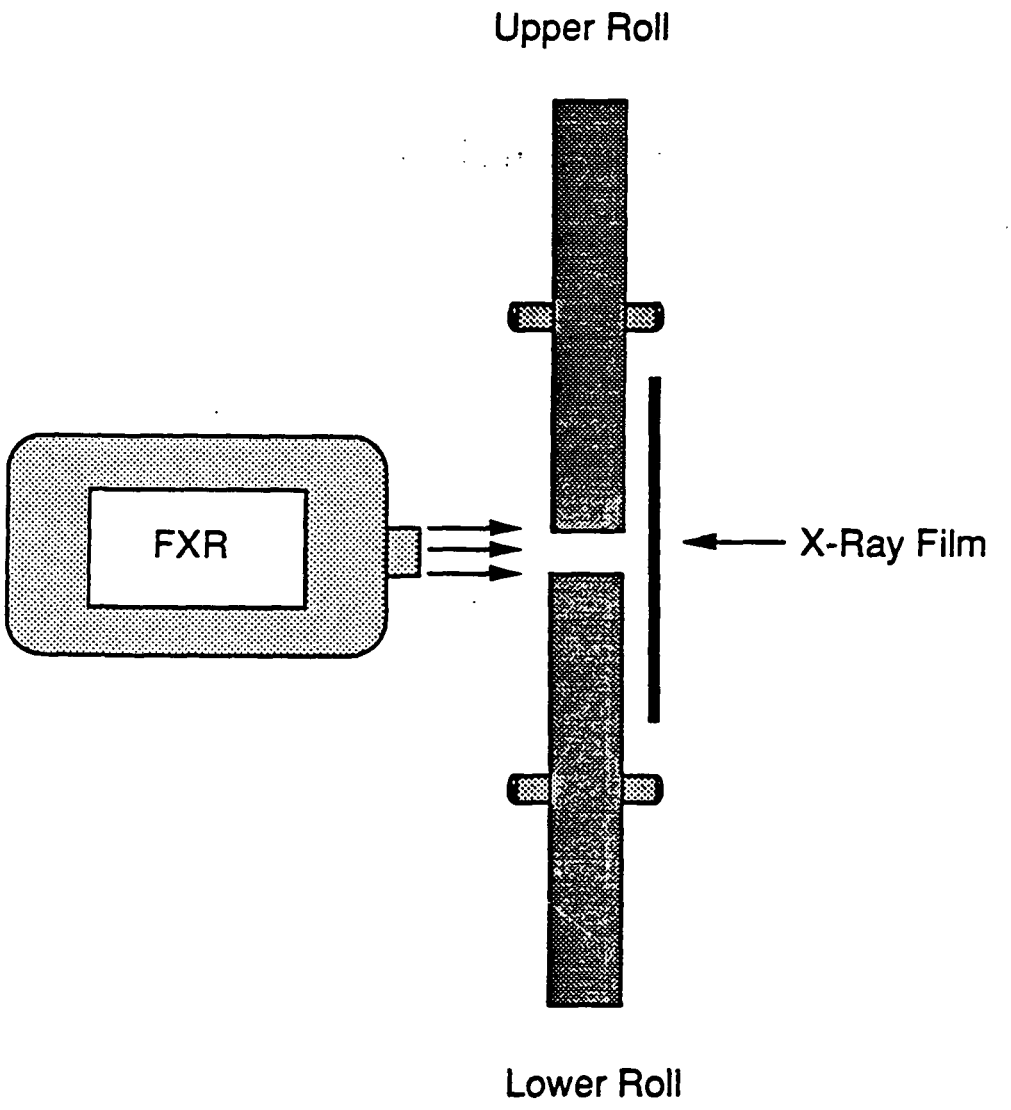

Figure 2. Schematic diagram of the relative position of the x-ray source, x-ray film, and the rolls.

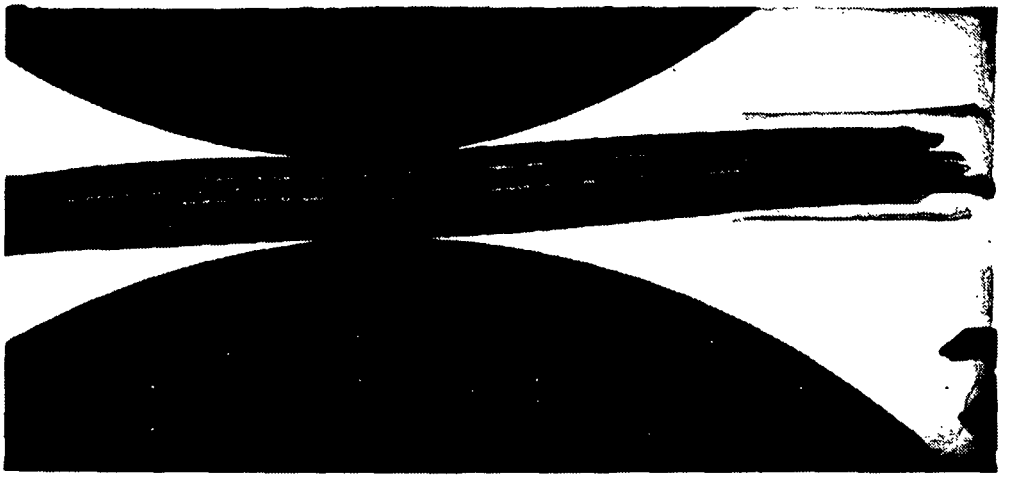

Figure 3a. Flash X-ray Radiograph of Target Particles (zero load).

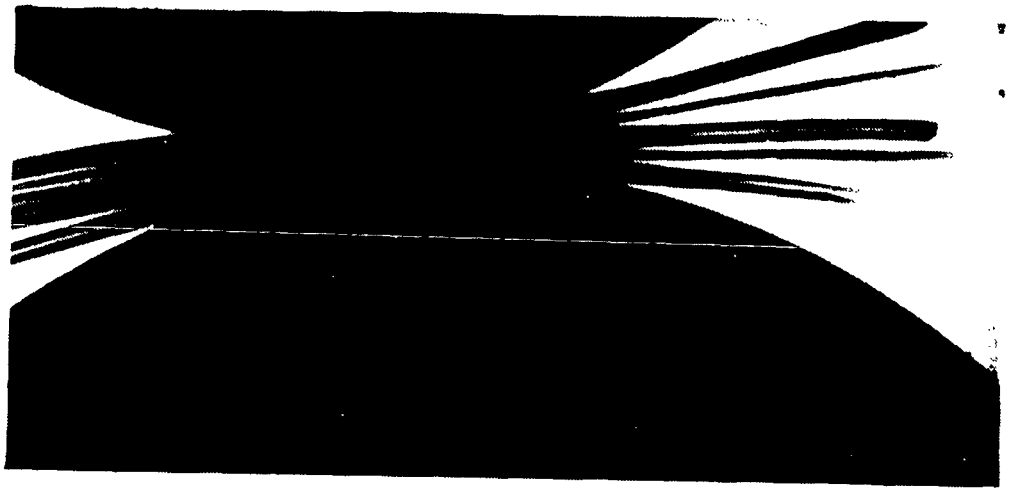

Figure 3b. Flash X-ray Radiograph of Target Particles (compressed).

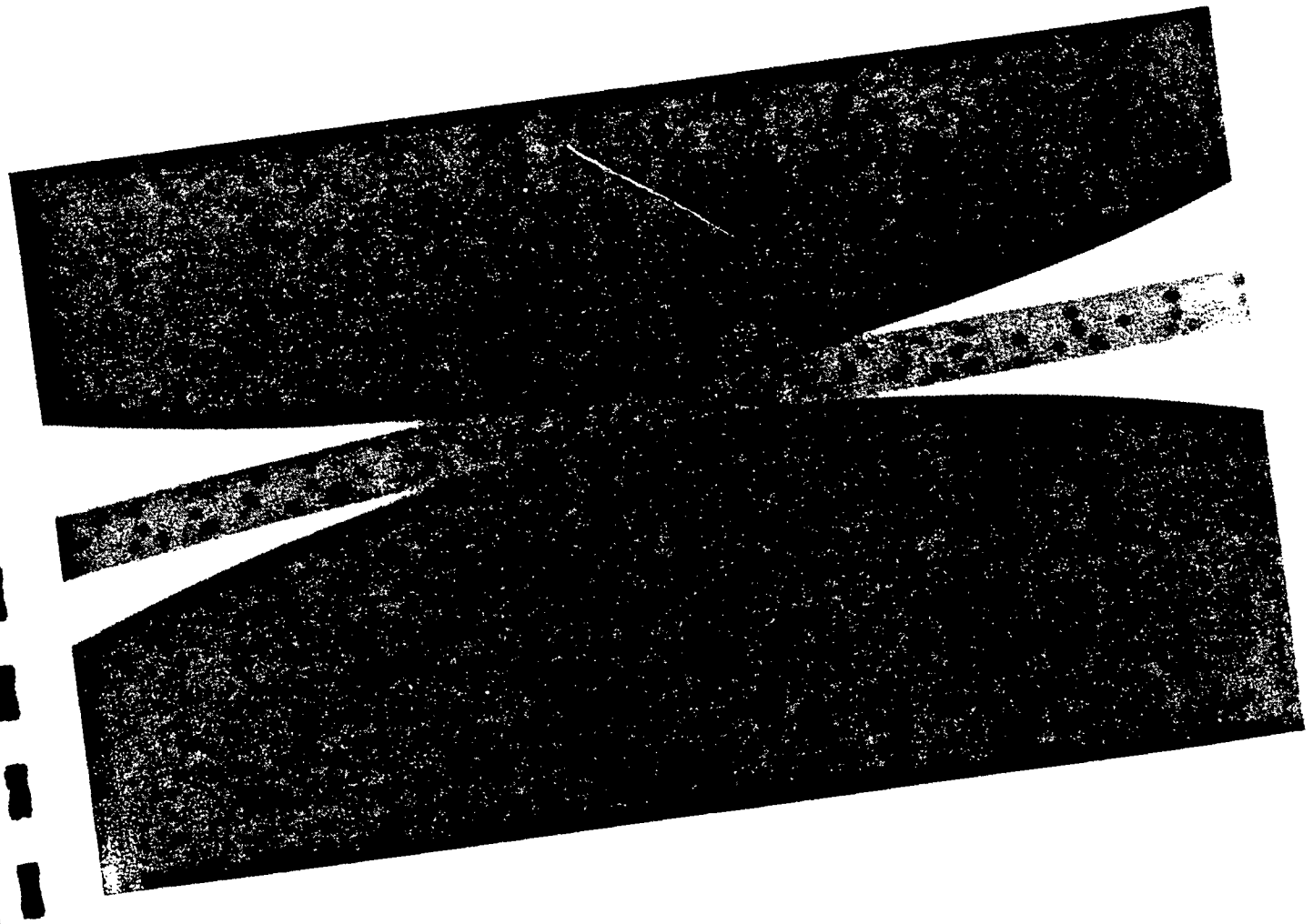

Figure 4. X-ray image of tracer particles in a deforming sheet.

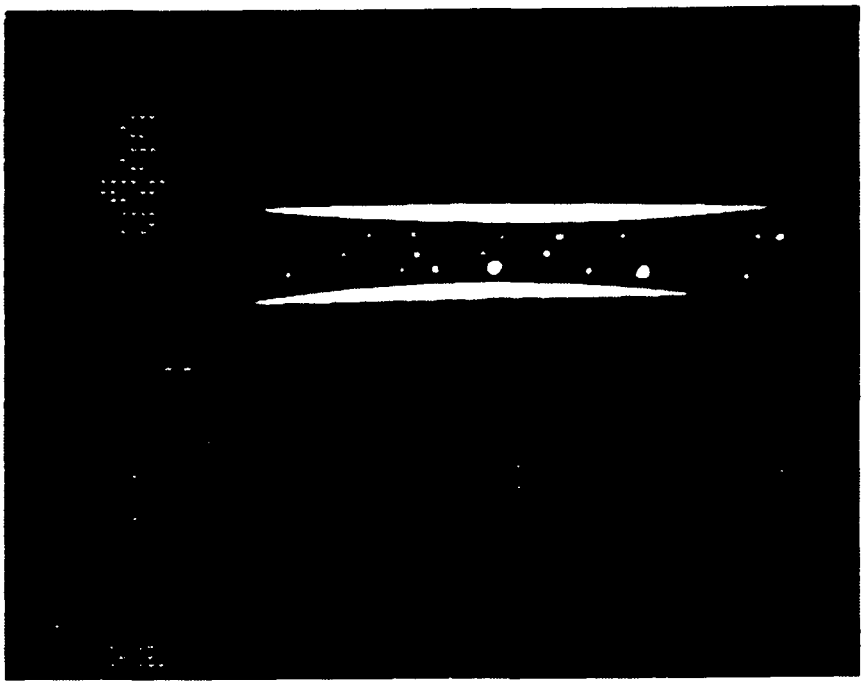

Figure 5. X-ray image of solid particle tracers in a sheet inside the nip of a roll press.

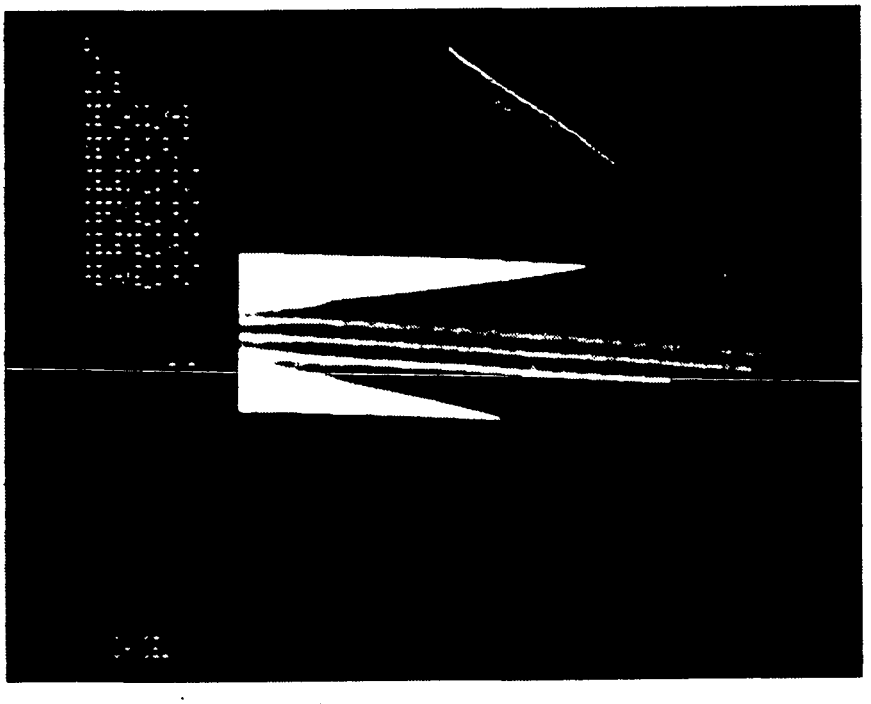

Figure 6. X-ray image of continuous tungsten wires in a sheet at the exit side of the nip.

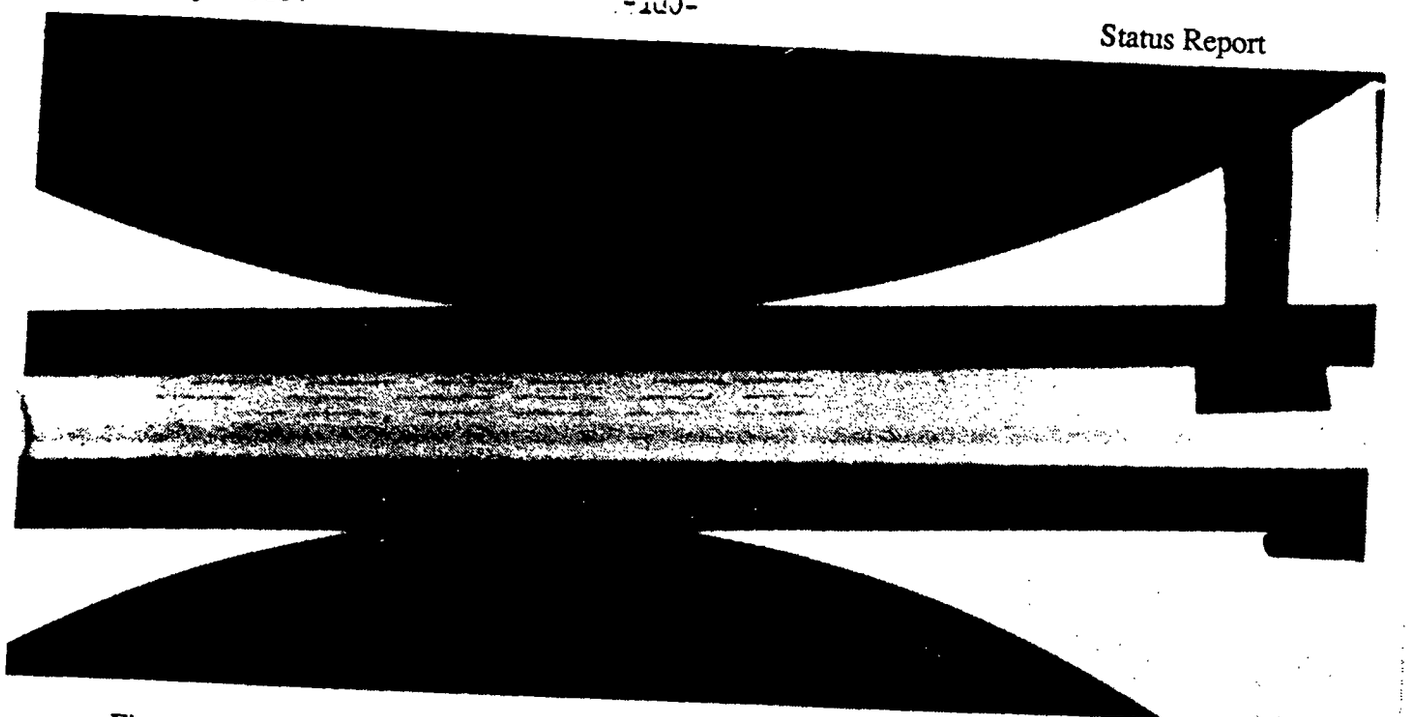

Figure 7. X-ray image of the sample under zero load (x5 magnification).

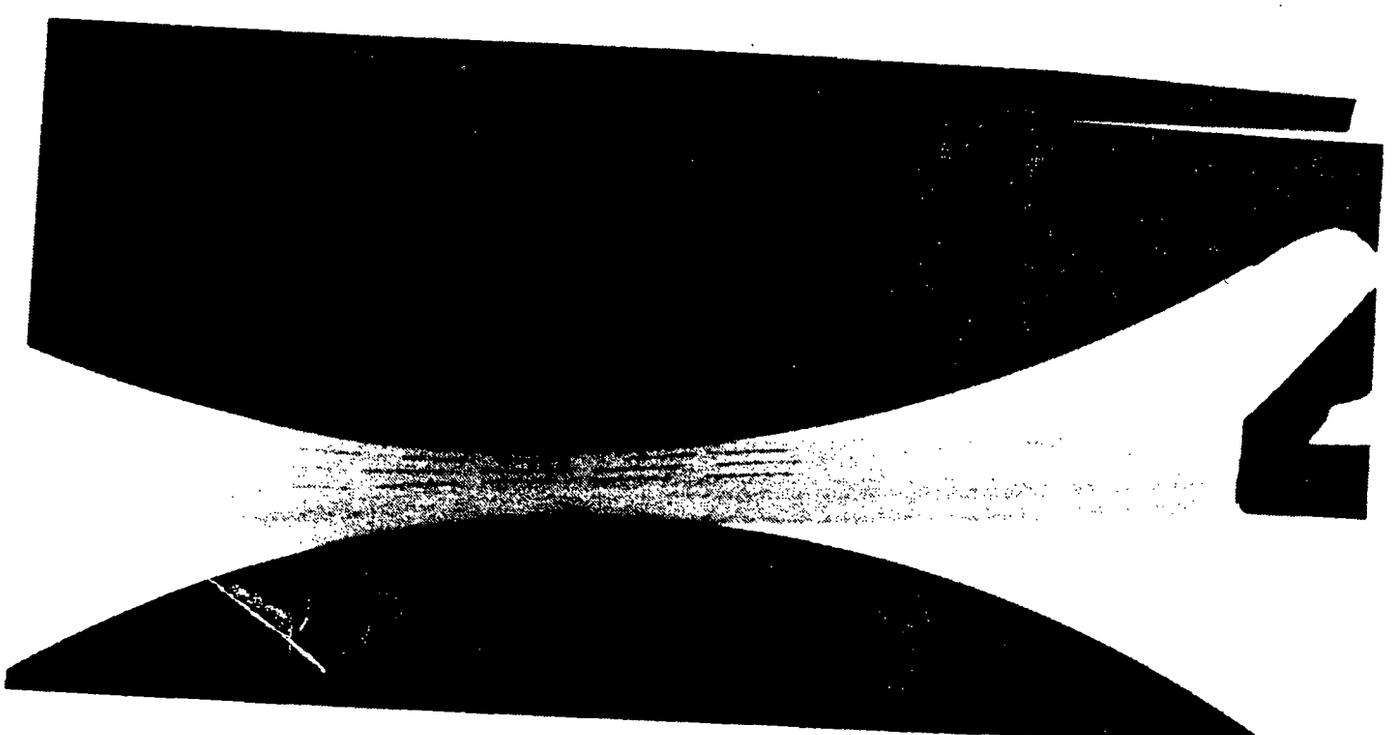

Figure 8. X-ray image of the sample at 685 psi and 100 fpm (x5 magnification).

CORROSION CONTROL IN BATCH DIGESTERS

STATUS REPORT

FOR

A NEW PROJECT

March 22, 1990

Institute of Paper Science and Technology
Atlanta, Georgia

PROJECT SUMMARY FORM

DATE: March 5, 1990

PROJECT: New Project - CORROSION CONTROL IN BATCH DIGESTERS

PROJECT LEADER: Per-Erik Ahlers

IPST GOAL:

Increase the life of batch digesters by proper selection of corrosion resistant materials.

OBJECTIVE:

To understand the causes of corrosion on stainless steel clad weldings as a basis for developing methods for reducing corrosion damage in kraft digesters. In addition, application methods for carbon steel digester claddings will be investigated as well as the identification of suitable cooking conditions.

CURRENT FISCAL BUDGET: New project (FY 90/91 $25,000)

PRIOR RESULTS: New Project

FUTURE PLANS:

Perform corrosion tests under conditions similar to those in the gas phase of batch digester during filling-up period by dripping synthetic white liquor on hot metal specimens of iron and nickel based alloys with various chromium content.

CORROSION CONTROL IN BATCH DIGESTER

New Project

THE PROBLEM STATEMENT

Corrosion conditions and corrosion rates in batch digesters vary depending upon the liquor composition, wood quality, cooking strategy, at the cooking vessel design and the structural materials. Normally the digesters are built of mild steel with some parts stainless steel such as the screen plates, valves and tube fittings.

The corrosion in carbon steel digesters can be characterized as uniform. That means, the internal surface remains passive or semi-passive, covered by corrosion products. However, amidst the passive area there are islands where corrosion is active for several cooking cycles before gradually approaching the passive state. The passive layer continues to grow slowly, and when it has reached a considerable thickness, the relatively brittle scale spalls off during the blow-down period, thereby activates the surface. As described, the localized areas are cyclically activated and passivated. The corroding areas can be considered as slowly moving islands, several feet in diameter. Over a long period of time this results in a relatively even corrosion pattern. The metal wastage is more accentuated on certain areas where the mechanical wearing and thermal fluctuations are higher.

In general, the corrosion rate seems to be sufficiently moderate, something between 0.1 and 0.3 mm/yr, which means a relative long lifetime for the digesters. However, in some cases, a higher corrosion rate is experienced, mostly in the upper part of the vessels. Overlay welding is a common practice to fill up the metal wastage in batch digesters. Different alloys besides carbon steel are used. The austenitic stainless steel grade AISI 309 is often used because it exhibits good corrosion resistant in kraft liquor environments. A disadvantage with this alloy is its different thermal expansion compared with the ferritic base metal, which can result in stress assisted failures.

Localized corrosion in the form of heavy pitting occurs in batch digesters on austenitic stainless steel weld claddings. Analyses of the metal composition and microstructure was

performed at IPST, but nothing unusual appeared. On some locations a slight chromium depletion was observed, but the chromium content was above 16% all samples. It is known that stainless steel is prone to cracking in a hot caustic environment, a phenomenon which is investigated largely in the nuclear power industry. The susceptibility of stress corrosion means an incomplete passivity or slow passivation process when activated. In cooking conditions, the metal potential is known to be low, close to the passive/active transition range. According to R.W. Staehle et al., stainless steel exhibits pronounced active/passive behavior in hydroxide solutions at 150°C and at a 20 mol/l concentration (Corrosion, Vol. 34, 1978, p. 413.). The occurrence of caustic stress corrosion at elevated temperatures is well established. Corrosion studies with 17Cr-13Ni stainless steel in 50% NaOH underwent active dissolution (G. Santarini and J.Y. Boss; Corrosion Sci., Vol. 19, 1979, p. 753). The sodium hydroxide concentration in the cooking liquor is roughly 5% or less corresponding roughly to 1 mol/l and consequently is not able to activate stainless steel without an increase in concentration.

Pitting and stress corrosion are closely related corrosion forms. Both are possible when the metal potential is within the borderline passivity region. In many cases the cracking process is initiated by pitting because surface pits acts as stress raisers. Under certain conditions the crack growth ceases due to the blunting effect on the crack tip, which normally results in a pit appearance damage.

A reason for the observed pitting corrosion on the welded stainless steel claddings could be that during the filling-up periods liquor splashes hit the hot digester wall, where the droplets will be concentrated and the passivity broken down locally. In addition, the boiling of the droplets and the associated thermal-shock might have some contributing effect. Also some organic acids, such as formic, acetic, and oxalic acids released from the wood of steam could promote activation of the metal.

In order to gain an understanding of the primary factors affecting local corrosion seen in practice, studies will be undertaken to clarify if an increase in concentration is possible under conditions prevailing in the filling period of a batch cook, what are the possible contributory factors, and what alloy will resist the aggravated conditions.

PROPOSED WORK

In order to investigate the corrosion resistance of various alloys, a series of stainless steel and nickel base metals should be exposed to conditions approximating those encountered during the start-up period of a cook. The temperature of corrosion specimens should be close the boiling point. Cool white liquor will be dripped on the hot metal surface in a moist environment in the presence and absence of organic acids.

Criterion for corrosion resistance will be metal wastage, the depth of the attack, and changes in the surface appearance.